PERSPECTIVE

Check for updates

Ferroelectric thin films: performance modulation and application

Shan Li,[a] Yilin Wang,[b] Mingdi Yang,[a] Jun Miao, [ID][a] Kun Lin,[a] Qiang Li,[a] Xin Chen,[a] Jinxia Deng[a] and Xianran Xing [ID] *[a]

Ferroelectric thin film materials have been widely applied in a great many fields for their robust spontaneous electric polarization and strong coupling with optical, electric and magnetic fields. In recent years, breakthrough progress has been made in the performance optimization and applications of these materials. Composition control and various types of strain can effectively regulate the performance of ferroelectric films, including ferroelectric hysteresis loop, Curie temperature, leakage current, *etc.*, to meet the application requirements of ferroelectric devices in various fields. Flexible ferroelectric thin film devices with excellent ductility and resilience have amazing application potential in intelligent robots, wearable electronic devices and the Internet of Things, expanding the application field of ferroelectric thin film materials. We briefly introduce the fabrication processes and application prototypes of flexible ferroelectric thin films. We conclude with limitations of existing research on ferroelectric thin film materials and suggestions for further research.

1. Introduction

Ferroelectrics are materials that possess spontaneous polarization without an external electric field, and the orientations of the polarization vector can be switched with the application of an electric field.[1] Thin-film ferroelectrics are important subjects of ferroelectric materials. The research on ferroelectric thin films can be traced back to the 1960s, when the development of semiconductor integration technology sparked interest in applying ferroelectric thin films to non-volatile memory devices. However, due to the immature thin-film preparation technology and the incompatibility of ferroelectric materials with semiconductor processes at that time, the research and application of ferroelectric thin-films progressed slowly. In the 1980s, the rapid development of ferroelectric thin film preparation technology broke the barrier of preparing high-quality ferroelectric thin films and laid the foundation for the development of ferroelectric thin film materials.[2,3] At that stage, various structural types of ferroelectric thin film materials were prepared and investigated, such as perovskite oxides, tungsten bronze and bismuth layered oxides.[4–6] Among them, perovskite-type oxide $Pb(Zr_xTi_{1-x})O_3$ (PZT) has attracted much

attention in research studies because of its superior ferroelectric and piezoelectric properties. With the rapid development of microelectronics technology, ferroelectric thin-film materials are added as functional components to microelectromechanical systems (MEMSs). In 1993, ferroelectric thin films were successfully integrated with Si complementary metal oxide semiconductors (CMOSs) and ferroelectric memory entered industrialization. From then on, the research on ferroelectric materials and devices has developed from single crystal devices to thin film devices, and from separate devices to integrated devices. In the following years, the application of pulsed laser deposition (PLD), magnetron sputtering, molecular beam epitaxy (MBE) and other technologies to prepare single crystal thin films has promoted research on the basic science of ferroelectric thin film materials such as $BiFeO_3$,[7] PZT,[8] and $BaTiO_3$.[9] With the continuous development of microelectronics technology and large-scale integrated circuits, the development trend of miniaturization, integration and light weight of electronic devices has appeared, and the requirements for ferroelectric devices have become higher and higher, which has stimulated the continuous development of ferroelectric thin films. So far, ferroelectric thin film materials have been widely used in many fields, such as memory devices, detectors, piezoelectric MEMSs, *etc.*[10–12]

With the rapid development of computational, modeling, synthesis, and characterization techniques, exotic physical phenomena and novel ferroelectric materials are constantly being discovered and explored. A superlattice is an epitaxial multilayer film structure obtained by alternately growing two or

[a] Beijing Advanced Innovation Center for Materials Genome Engineering, Institute of Solid State Chemistry, University of Science and Technology Beijing, Beijing 100083, China

[b] Institute of Advanced Materials (IAM), Jiangsu National Synergetic Innovation Center for Advanced Materials (SICAM), Nanjing Tech University, 30 South Puzhu Road, Nanjing, 211816, China. E-mail: xing@ustb.edu.cn

more different thin film materials, which is an effective approach to obtain excellent properties and explore new physical phenomena. The strong polarization enhancement was achieved in a three-component superlattice $BaTiO_3/SrTiO_3/CaTiO_3$.[13] By controlling the volume fraction of $PbTiO_3$, the polarization value and Curie temperature can be adjusted over a wide range in the $PbTiO_3/SrTiO_3$ superlattice[14] and the recovery of ferroelectricity was observed in the ultrashort period superlattice $(PbTiO_3)_1/(SrTiO_3)_1$.[15] In ferroelectric–paraelectric superlattices, exotic physical phenomena can also be induced, such as vortex/anti-vortex structures,[16] ferroelectric skyrmions[17] and negative capacitance.[18] In 2011, promising ferroelectric, Si-doped HfO_2 ferroelectric thin films were reported by T. S. Böscke et al.,[19] which opened the exploration of HfO_2-based ferroelectric thin film materials. Although the origin of ferroelectric properties is still ambiguous, HfO_2-based ferroelectric thin film materials with the advantages of simple composition elements, low dielectric constants, good ferroelectric properties even at the nanometer scale, and full compatibility with silicon semiconductor processes are expected to be applied in high-performance microelectronic devices in the future.[20–22]

Ferroelectric thin film materials have broad application prospects in many fields, but there are very few ferroelectric thin film devices that can be commercialized at present, because the performance of many ferroelectric thin film materials cannot meet the requirements of commercialization. Large leakage current, low nanoscale polarization value, low piezoelectric coefficient, poor cycling stability, thermal stability, etc. are the factors hindering the commercialization of ferroelectric thin film devices. Therefore, improving the performance of ferroelectric thin films is a problem to be solved in the application field of ferroelectric thin film materials. In this Review, based on the excellent work published, we introduced the rational modulation approaches for the properties (Section 2), and the application field (Section 3) of ferroelectric thin film materials. Flexible ferroelectric thin films are free from the constraint of the substrate and have excellent ductility and resilience, expanding the application fields of ferroelectric thin film materials. The fabrication processes and application prospects of flexible inorganic ferroelectric thin film materials are presented in Section 4.

2. Performance optimization

Ferroelectric thin film materials have wide application prospects in a lot of fields, but different scenarios have different requirements for performance. For example, ferroelectric memory requires superior fatigue resistance and ferroelectric sensors need robust spontaneous polarization. Hence, it is necessary to flexibly adjust the performance of ferroelectric thin film materials. In this section, we introduce some common methods for adjusting ferroelectric thin film properties.

2.1 Composition control

Composition control is the most common and easiest approach to modify the structure and the properties of ferroelectric thin films. Here we review some of the effects of chemical composition control on the properties.

2.1.1 Modify the polarization value (the P–E hysteresis loops). In ferroelectric sensors, large remanent polarization values (P_r) result in a higher sensitivity, so the higher the P_r, the better. The P_r value of (001)-oriented $NaNbO_3$ thin films adjusted by Co, Mn and La co-doping is 31 μC cm^{-2}, which is approximately three times that of the unmodified $NaNbO_3$ thin films (10 μC cm^{-2}).[23] In La-doped PZT (PLZT) thin films, the P_r value varies with the amount of La dopant and the maximum P_r of 91 μC cm^{-2} (almost twice that of the pure PZT thin films) was realized in 0.5 at. % PLZT thin films.[24] Ferroelectric or antiferroelectric thin film materials can be applied to electrostatic energy storage. Narrow P–E curves are beneficial for improving energy storage density and efficiency (the detail about energy storage is discussed in Section 3.2). As shown in Fig. 1a, doping Sm in $BiFeO_3$–$BaTiO_3$ (BFO–BTO) relaxation ferroelectric films can significantly narrow the P–E loop, and achieve superparaelectric relaxation ferroelectrics with high energy storage density and efficiency.[25]

2.1.2 Improve fatigue resistance. Polarization fatigue is the phenomenon in which the switchable polarization gradually decreasees under increasing number of electrical cycling, which is one of the major issues affecting the working life of ferroelectric devices. For $PbZr_{0.3}Ti_{0.7}O_3$ thin films, the switchable polarization values began to decrease after 10^7 cycles and decreased by approximately 50% after 10^{10} cycles; the switchable polarization of Mn (0.5–1 mol%) doped $PbZr_{0.3}Ti_{0.7}O_3$ films decreased by 2–3% after 10^{10} cycles;[29] no fatigue was observed in Nb and Si co-doped $PbZr_{0.2}Ti_{0.8}O_3$ thin films, even after 10^{10} cycles.[30] Fig. 1b shows cyclic fatigue tests for energy storage density and efficiency of $(0.55 - x)$BFO–xBTO–0.45STO solid–solution thin films with various x values. It can be seen that the $x = 0$ thin film broke down after 10^6 charge–discharge cycles, while negligible fatigue ($< 3\%$) after 10^8 cycles was observed in BTO-doped films.[26]

2.1.3 Reduce leakage current. The leakage current causes ferroelectricity deterioration, self-heating and reliability problems, which hinders the practical applications of ferroelectric thin films. Element doping can inhibit the formation of oxygen vacancies, thus reducing the leakage current and improving the ferroelectric property of the thin film.[31,32] Doping with 0.08 mol $BiFeO_3$ in $Bi_{3.25}La_{0.75}Ti_3O_{12}$ thin film can reduce the leakage current density by two orders of magnitude and increase the breakdown strength from 2001 kV cm^{-1} (pure $Bi_{3.25}La_{0.75}Ti_3O_{12}$) to 3316 kV cm^{-1} (Fig. 1c), which allows high electric fields to be applied onto the films to produce large polarization, resulting in higher energy storage densities.[27]

2.1.4 Thermal stability. The high Curie temperature and thermal stability enable ferroelectric thin film devices to operate at high temperature. During room temperature to 100 °C, a temperature-independent polarization behavior was observed in the $PbTiO_3$–$BiMg_{0.5}Ti_{0.5}O_3$ and $PbTiO_3$–$FeNdO_3$ thin films.[33,34] The energy storage density (40 J cm^{-3}) and efficiency (80%) of the 5.6 mol% Si-doped HfO_2 thin films were maintained over a wide temperature range (25–175 °C).[35]

Fig. 1 (a) The $P–E$ curves of Sm-doped BFO−BTO thin films with various Sm content.[25] (b) A cyclic fatigue test for energy storage density and efficiency of $(0.55 − x)$BFO−xBTO−0.45STO solid−solution thin films with various x values.[26] (c) The breakdown strengths of BLT−xBFO thin films were analyzed by two-parameter Weibull distribution.[27] (d) Photocurrent density−voltage curves of La-substituted BFO films.[28]

2.1.5 Regulate ferroelectric-related properties. The Ti/O deficiency can drive a phase transition from paraelectric to ferroelectric in $SrTiO_3$ thin films.[36] In Na-deficient $NaNbO_3$ thin films, Na defects drive the formation of out-of-phase boundaries between the nanopillar regions and matrix regions, which is responsible for the huge piezoelectric response.[37] A large ferroelectric resistance switching with an ON/OFF rate (12 000) comparable to that of ferroelectric tunnel junctions was observed in Sm doped $BiFeO_3$ thin films.[38] The 1 mol% Mn-doped $PbZr_{0.3}Ti_{0.7}O_3$ thin films showed an enhanced pyroelectric effect.[39] The substitution of Pb by Sm in $PbZr_xTi_{1−x}O_3$ thin films resulted in an unusually large piezoelectric coefficient near the Curie temperature.[40] The phase transition from the polar ferroelectric phase to a nonpolar paraelectric phase exists in $BiFeO_3$ thin films modified by rare-earth metals (La Sm, Gd, Dy), and substantial enhancement of ferroelectric photovoltaic (Fig. 1d) and electromechanical properties were observed near the phase boundaries of the nonpolar and polar phase.[28,41,42]

2.1.6 Introduce other properties. Multifunctional materials can be obtained by doping special ions in ferroelectric thin films. Single-phase multiferroic thin films at room temperature can be prepared by introducing magnetic elements (Fe, Co, Mn, etc.) into ferroelectric thin films.[43] For example, Mn-doped $BaTiO_3$ thin films,[44] and Sm and Fe co-doped $PbTiO_3$ thin films.[45] Through inserting luminescent centers into ferroelectric thin films, high-performance optical materials were

constructed, such as Er/Yb co-doped $BaTiO_3$ thin films[46] and Ni-doped $Ba_{0.5}Sr_{0.5}TiO_3$ thin films.[47]

Compositional modulation can change the chemical and defect structure of materials, and plays an important role in the regulation of ferroelectric material properties, such as remanent polarization, leakage current, fatigue, and piezoelectric properties, etc. The chemical method is a universal application to modify kinds of ferroelectric thin films grown on various substrates. However, as the chemical substitution could provide limited "internal pressure", the properties can only be modified in a narrow range. Moreover, although there are many methods for preparing thin films, few can achieve precise control of composition, and many preparation methods are not suitable for preparing thin films with complex chemical compositions.

2.2 Strain engineering

In ferroelectric materials, there is a strong coupling relationship between polarization and strain, which can be used to tailor the properties of materials.[48,49] In the early 1950s, researchers studied the influence of hydrostatic pressure on the Curie temperature and dielectric properties of ferroelectric ceramics and single crystal materials.[50–52] Normally, the bulk material can withstand less than 0.1% compressive and tensile strain, while thin films can tolerate approximately several percent of biaxial strain.[53] The high stress tolerance of thin film materials provides a broad platform for strain control

performance. The strain engineering of ferroelectric thin films has developed rapidly in the last ten decade.[54-56] In particular, the construction of a stress-phase diagram (the relationship between the ferroelectric domain structure and strain) provides a good foundation for ferroelectric strain engineering. There are many ways to apply strain in thin films. Here, we briefly introduce the development of several types of strain on the properties of ferroelectric thin films.

Biaxial strain arises from the lattice mismatch between the film and the substrate, and is defined as:

$$\varepsilon = \frac{a_s - a_f}{a_s}$$

where a_f and a_s are the lattice parameters of the thin films and substrate, respectively.[53] The alteration of biaxial strains can be realized by altering the type of substrate, it is the most convenient and widely used method in strain engineering. As shown in Fig. 2a and b, the Curie temperature and ferroelectric polarization value of the $BaTiO_3$ thin films can be tuned by changing the substrates.[9] A similar situation occurs in several perovskite ferroelectric thin film materials, such as $PbTiO_3$, $BiFeO_3$, and $LiNbO_3$.[57] Biaxial strain can be used to drive phase transition. Bulk STO is paraelectric, and ferroelectricity can be realized by depositing thin films on suitable substrates.[58] In

$Hf_{0.5}Zr_{0.5}O_2$ thin films, a ferroelectric rhombohedral phase can be obtained by applying the biaxial compressive strain.[59] A phase transition from the M_A phase to the M_B phase occurs in $BiFeO_3$ thin films as the epitaxial strain changes from low mismatch compressive strain to tensile strain.[60] The monoclinic BFO films show a high P_r (55 μC cm^{-2}), which is an order of magnitude higher than that of the bulk.[61] In the case of high compression strain (> 4.5%, $LaAlO_3$ substrate), low-symmetry rhombohedral phases and tetragonal-like phases coexist in $BiFeO_3$ thin films (Fig. 2c).[7,62] The mix-phase structure is similar to the morphotropic phase boundaries (MPB) and the improved electromechanical responses have been certified in the mix-phase region.[63] The elastocaloric effect of $BaTiO_3$ thin films can be regulated by the use of different compressive substrates.[64]

Because of the clamping of the substrate, epitaxial strain can only be maintained within the critical thickness, restricting the efficiency of the biaxial strain in rather thick film. Due to the limitation of a high-quality single crystal substrate type, a continuously adjustable biaxial strain state cannot be achieved.

Vertical strain comes from the vertical lattice mismatch of the two materials, as shown in Fig. 2d. Vertical strain runs through the entire film thickness and could apply strain in the thick film.[67] For tetragonal perovskite ferroelectric materials,
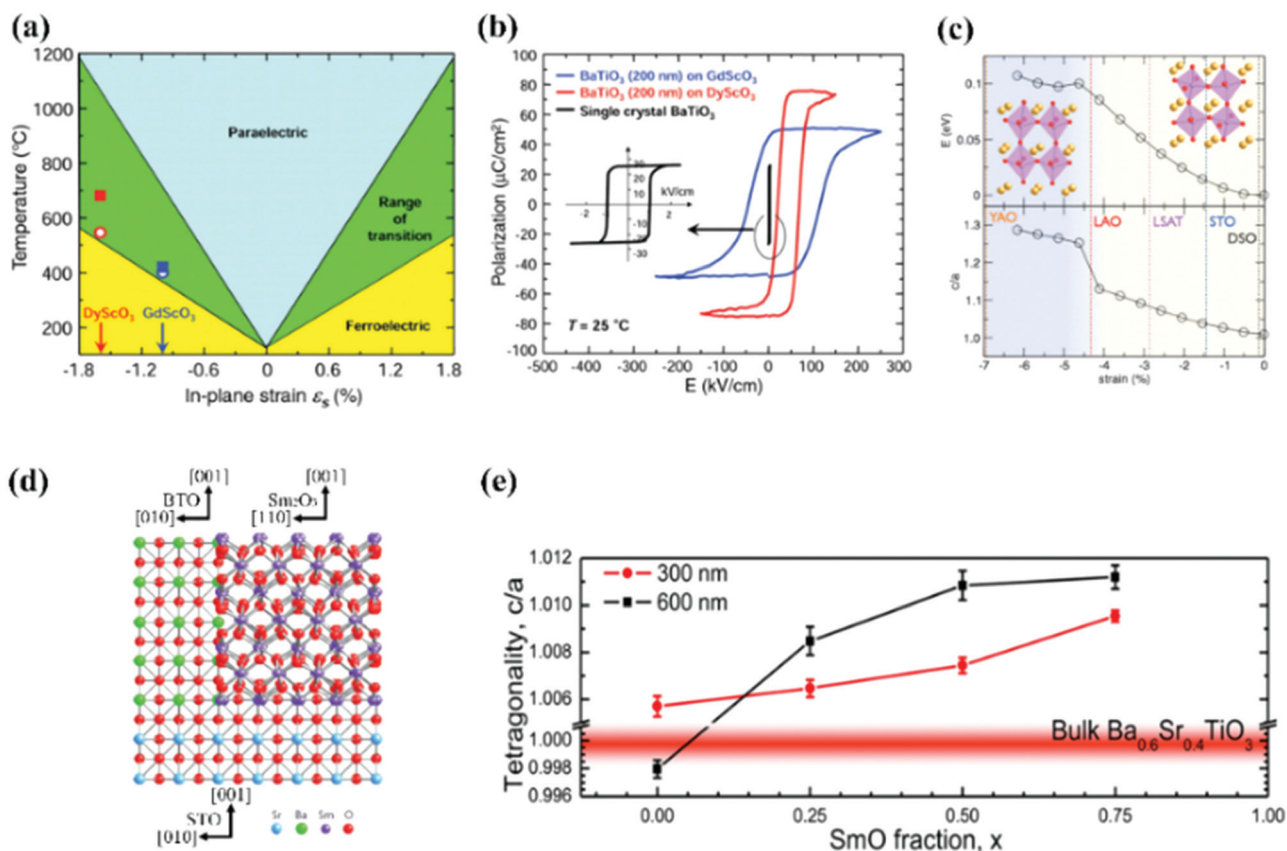

Fig. 2 (a) Misfit strain–temperature phase diagram of BTO and (b) P–E hysteresis loops of BTO thin films grown on different substrates.[9] (c) Evolution of the energy (top) and c/a ratio (bottom) as a function of misfit strain for BFO thin films.[7] (d) Schematic crystallographic model of vertical strain between Sm_2O_3 and BTO.[65] (e) Tetragonality (c/a ratio) in BSTO thin films *versus* Sm_2O_3 content.[66]

the ferroelectric performance is closely related to the axial ratio. Vertical strain without constraint of the substrate can have a significant influence on the tetragonality of materials; therefore, vertical strain is an effective way to tune the performance of perovskite ferroelectric materials.[65] Many rare-earth oxide, spinel and metal–oxide nanopillars were successfully assembled with perovskite oxide to achieve various properties. For example, the d_{33} (longitudinal piezoelectric coefficient) value of the $0.5BaTiO_3:0.5Sm_2O_3$ vertical composite thin films (45–50 pm V^{-1}) is higher than that of pure $BaTiO_3$ thin films and can be maintained from room temperature to 250 °C, which comes from the vertical tensile strain tuned by Sm_2O_3 nanopillars.[68] In the $(Ba_{0.6}Sr_{0.4}TiO_3)_{0.25}:(Sm_2O_3)_{0.75}$ thin films, $Ba_{0.6}Sr_{0.4}TiO_3$ is subjected to vertical tensile strain controlled by Sm_2O_3, and the tetragonality increases with increasing thickness and Sm_2O_3 content (Fig. 2e).[66] In the 600 nm thick film, pure $Ba_{0.6}Sr_{0.4}TiO_3$ is fully relaxed, while the composite film maintains good tetragonality (c/a = 1.0112). Ferroelectric properties can be induced by vertical strain in conventional non-ferroelectric materials. In composite films composed of MgO nanopillars and a $SrTiO_3$ matrix, vertical tensile strain can be applied to the $SrTiO_3$ lattice to achieve tetragonal distortion and induce ferroelectricity.[69] $SrTiO_3:Sm_2O_3$ nanocomposite thin films have been confirmed to be ferroelectric and have

the merits of high dielectric tunability (49%), low dielectric loss (less than 0.01) and a high commutation quality factor (over 2800) at room temperature, making $SrTiO_3:Sm_2O_3$ nanocomposite thin films suitable for microwave tunable devices.[70] In vertical nanocomposite heteroepitaxial films, magnetic nanopillars with magnetostriction properties are embedded in the ferroelectric matrix, and a strong magnetoelectric coupling effect can be realized by a vertical strain coupling mechanism,[71] including $BaTiO_3:CoFe_2O_4$ nanostructures[72] and $BiFeO_3:CoFe_2O_4$ nanocomposites,[73,74] etc.

Interphase strain – Two materials with resemblant crystal structures but unequal lattice parameters were assembled into a single epitaxial composite with the same lattice constant and well-matched interface, and the strain generated at the boundaries of the two kinds of materials is the interphase strain (Fig. 3a). Interphase strain was first proposed and reported by Zhang et al. in 2018.[75] Fig. 3b shows the synchrotron X-ray RSMs around the (103) plane of the films and substrates. By introducing the PbO phase into a $PbTiO_3$ epitaxial thin film, the out-of-plane crystal parameter c of the PTO composite thin films shows substantial increase, resulting in an axial ratio as large as 1.238 (that of bulk is 1.065[76]). The P_r value of ultra-tetragonal $PbTiO_3$ epitaxial composite films is 236.3 μC cm^{-2} (Fig. 3c), which is the largest value reported to date.[62] Similar
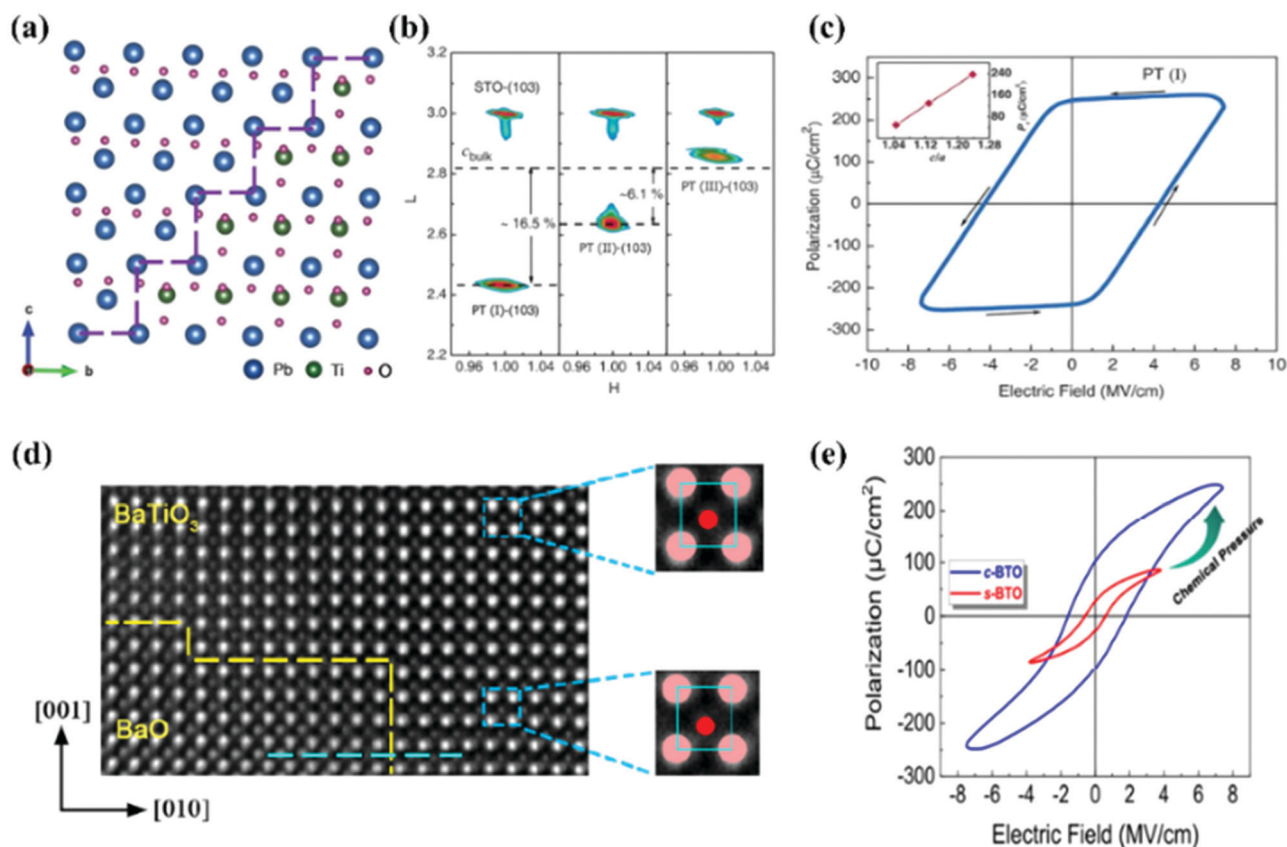

Fig. 3 (a) Crystallographic model of interphase strain between PTO and PbO; (b) Synchrotron X-ray reciprocal space mappings (RSMs) study of PT(I), PT(II), and PT(III) epitaxial thin films around the STO (103) plane, and (c) P–E hysteresis loops of ultra-tetragonal PTO thin films;[75] The cross-sectional HAADF-STEM (d) and P–E hysteresis loops (e) of c-BTO films.[76]

structures were also obtained in $BaTiO_3$:BaO epitaxial composite films (c-BTO).[77] The cross-sectional HAADF-STEM image (Fig. 3d) of c-BTO shows that $BaTiO_3$ and BaO have a coherent interface and that interphase strain exists between them. By calculation, the BaO lattice exerted a chemical negative pressure of -5.7 GPa on the $BaTiO_3$ lattice, resulting in the largest tetragonal distortion ($c/a = 1.12$), and the P–E loops of the c-BTO (Fig. 3e) exhibit the largest P_r value of 100 μC cm^{-2} in $BaTiO_3$ materials. Surprisingly, ferromagnetism was observed in the ultra-tetragonal $PbTiO_3$ composite film. The saturation magnetic moment of 10 nm thick composite films deposited on the $LaAlO_3$ substrate is 55 emu cc^{-1}.[78] Interphase strain can not only induce negative chemical pressure to improve ferroelectric performance but also provide a new method for the design and exploration of multiferroic materials.

The freestanding membrane is free from the clamp of the substrate which provides a new direction for exploring the structure and properties of ferroelectric film materials. High-quantity freestanding perovskite membranes can be synthesized by the use of a sacrificial water-soluble layer ($Sr_3Al_2O_6$).[79,80] The perovskite thin films are deposited on substrates with $Sr_3Al_2O_6$ buffer layers and placed in deionized water to remove the buffer layer, finally, transferring the membrane to the desired substrate.[79] Free from the constraints of the substrate, perovskite ferroelectric membranes may exhibit some unexpected structures and properties. For example, $BaTiO_3$ membranes show superelasticity and ultraflexibility.[81] Generally, oxide ferroelectric materials are brittle, whereas a 120 nm thick $BaTiO_3$ membrane can bear up to 10% of the mechanical bending strain without any crack, and the strain state can be recovered immediately when the 60 nm thick membrane is bent at an angle of 40° (Fig. 4a). Even when the

bending angle is increased to 80°, a large part of the strain can be recovered instantly, which demonstrates the superelasticity and ultraflexibility of $BaTiO_3$ membranes. The structural transition from an R-like phase to a T-like phase with the removal of a substrate, occurs in freestanding $BiFeO_3$ membranes with less than four unit cells (Fig. 4b and c).[82] As the thickness decreases, the axial ratio of $BiFeO_3$ membranes increases, and the 3 unit cells of $BiFeO_3$ membranes exhibit a remarkably large axial ratio (1.22), which is comparable to the epitaxial strain-driven T-like phase $BiFeO_3$ thin films.[62,83]

The realization of composition control and strain engineering depends on the deposition method and thermal treatment process of the thin films. The chemical composition, defect structure and strain state of the thin films can be flexibly controlled by different deposition methods and thermal treatments, so as to achieve the adjustment of the properties. Nowadays, many deposition methods are applied to grow ferroelectric thin films. Classified by the mechanisms, the deposition methods are divided into two categories: chemical methods and physical methods. Chemical methods, including chemical solution deposition (CSD, also called sol–gel), chemical vapor deposition (CVD), *etc.*, have strong advantages in composition regulation and are suitable for preparation of ferroelectric thin films with complex chemical composition,[84,85] which can flexibly and precisely control the chemical composition. Simple instruments and easy experimental processes make chemical methods appealing. However, chemical methods generally grow polycrystal thin films, whereas physical methods are much more appealing to grow epitaxial thin films. The properties of thin films prepared by chemical methods are greatly affected by the thermal treatment process.[86] Physical methods, such as atomic layer deposition
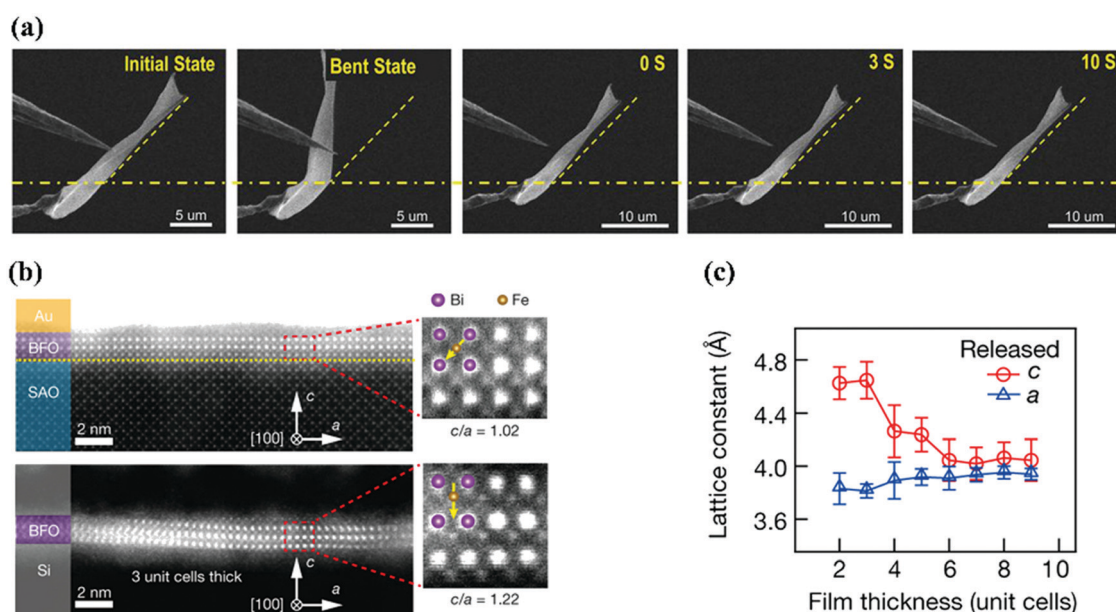

Fig. 4 (a) SEM images of the bending and recovery process at a bending angle of 40° for a BTO nanobelt.[79] (b) Cross-sectional HAADF-STEM images of a BFO thin film (three unit-cell) before (top) and after (bottom) separation from the substrate and (c) the crystal parameters a and c as a function of the freestanding BFO film thickness.[80]

(ALD), pulsed laser deposition (PLD), molecular beam epitaxy (MBE), and magnetron sputtering (MS), are widely applied to prepare high-quality ferroelectric thin films, including superlattices and ultrathin films, as these methods can *in situ* control the growth of crystal on an atomic level and accurately control the thickness of the film. Compared with MBE and ALD methods, MS and PLD methods have the advantage in flexible control of chemical composition and can be used to prepare the epitaxial thin films with complex compositions.[36,75] The equipment of ALD and MBE are expensive, and the preparation conditions are difficult to achieve; MS can achieve large-scale preparation, but PLD cannot. These methods have different advantages and disadvantages. In order to obtain films with specific structures or properties, flexible selection of appropriate thin film deposition methods is required.

3. Application

3.1 Nonvolatile random-access memory

Ferroelectric random-access memory (FeRAM) is one of the main application fields of ferroelectric thin film materials.[87] In FeRAM, two opposite polarization states of ferroelectric thin films are used for data storage.[88] FeRAM has the merits of nonvolatility, fast running speed, low power consumption and irradiation resistance. FeRAM can be divided into TC-type FeRAM (including 1T1C, 2T2C, 1T2C, T: transistors, C: capacitors) and 1T-type FeFETs (ferroelectric field effect transistors) according to different storage unit structures.

TC-type FeRAM works through the charge storage effect of a ferroelectric capacitor and the structure schematic diagram of the 1T1C-type FeRAM is shown in Fig. 5a.[88] During the "write" operation, the polarization direction of the ferroelectric film change with the polarity of the applied electric field. Due to the self-generating stability of ferroelectric remanent polarization, the polarized charge accumulates on the electrode of the ferroelectric capacitor after removal of the applied electric field, and the two electrical properties of polarized charge are used to represent two logical states of 0 and 1. In the "read" operation, the readout voltage is applied to the ferroelectric capacitor, and the polarization reversal is judged by comparing the output current with the reference current, to determine the electrical properties of the stored charge in the ferroelectric capacitor. During this operation, the polarization direction of the ferroelectric capacitor whose polarization direction is different from the polarity of the read operation voltage, transforms to the opposite direction, which destroys the original storage state. Therefore, after the read operation, the information must be written back to restore the original storage state of the storage unit. Because the "read" process of TC-type FeRAM is destructive, the cyclic fatigue characteristics of ferroelectric films are needed.

Ferroelectric thin films applied in TC-type FeRAM require a high remanent polarization value, low coercive voltage and saturation polarization voltage, suitable Curie temperature and good fatigue resistance. At present, PZT- and $SrBi_2Ta_2O_9$ (SBT)-based ferroelectric thin film materials are used in commercial FeRAM.[89] SBT-based thin film materials have the advantage of excellent fatigue resistance.[90,91] SBT-based memory has good cyclic stability and even shows a fatigue-free phenomenon after 10^{11} switching cycles.[92] However, the low storage density due to the intrinsic low remanent polarization value ($2P_r$:15–20 μC cm^{-2}), and the high integration temperature (700–800 °C) limit the development of SBT-based FeRAM.[93,94] Due to the outstanding ferroelectric performance and low integrated temperature (600 °C), PZT-based ferroelectric thin films are widely used in FeRAM.[95] Nevertheless, the fatigue resistance of the PZT film is poor. With the increase in the read/write cycle, a polarization decrease usually occurs at 10^6 cycles, which is far less than the requirement of commercial memory (10^{10}, or even higher in special cases).[94] The fatigue resistance of PZT-based capacitors can be optimized to 10^{11} by applying oxide electrodes (such as $LiNiO_3$, $SrRuO_3$, RuO_2)[96,97] or doping elements (such as Si, Nb, Mn),[29,30] enabling the commercialization of PZT-based FeRAM.

The PZT-based embedded FeRAM technology node stagnates at 130 nm[98,99] which is an order of magnitude larger than DRAM. This is due to the size effect of the perovskite ferroelectric materials. As the size of the capacitor (ferroelectric thin film thickness) decreases, the polarization value of the ferroelectric film declines, resulting in a decrease in the measurable storage charge on the electrode. According to the calculation, the remanent polarization values required for FeRAM with a stacked planar capacitor utilizing a 90 nm technology node are $2P_r > 84$ μC cm^{-2}.[100] Although the P_r value of PZT is as large as 100 μC cm^{-2},[101] the polarization value of PZT in FeRAM prepared by the semiconductor process is less than 40 μC cm^{-2}. To reduce the technology nodes and improve the storage density, 3D capacitors are used instead of 2D planar capacitors to compensate for the area loss.[102] The schematic drawing of 2D and 3D capacitors are shown in Fig. 5b.[103] Yeh *et al.* prepared 3D PZT-based capacitors with ferroelectric properties comparable to planar devices in the laboratory.[104] However, it is extremely difficult for PZT to form ferroelectric phases on sidewalls, and the idea of improving the storage density of PZT-based FeRAM by integrating 3D capacitors is still in the laboratory phase. In 2011, the discovery of HfO_2-based ferroelectric materials[19] made it possible to reduce the size of FeRAM. In 2014, Polakowski *et al.* reported 3D trench capacitors with Al-doped HfO_2 thin films as ferroelectric layers.[103] The P_r value based on the plane-projected area of
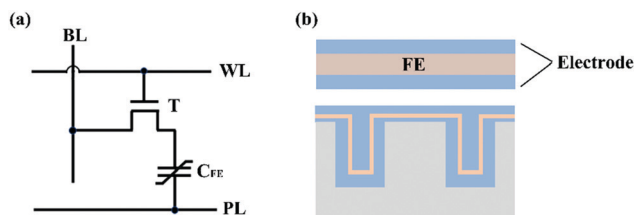

Fig. 5 (a) Structure schematic diagram of the 1T1C-type FeRAM. (b) The schematic diagram of two-dimension (2D) planar capacitors (top) and two-dimension (3D) deep trench capacitors.

the 3D trench capacitors with 100 k trenches is 152 μC cm^{-2} and the actual P_r value is 13.6 μC cm^{-2} which is similar to that of the 2D planar capacitor (15 μC cm^{-2}), suggesting that any parts, including the sidewalls of the trenches, contribute to the entire polarization value. In 2019, the TiN/Hf$_{0.5}$Zr$_{0.5}$O$_3$/TiN ferroelectric capacitor was successfully integrated into the 130 nm technology node back-end-of-line (BEOL) by T. Francois et al.[105] The capacitor exhibited excellent performance: 30 ns operation speed, $2P_r > 40$ μC cm^{-2}, and endurance > 10^{11} cycles at 4 V applied voltage. HfO$_2$-based ferroelectric materials have excellent ferroelectric properties in 3D capacitors and can be compatible with silicon CMOS (complementary metal oxide semiconductor) processes, so they are the candidate material for a new generation of FeRAM.[20,106] However, a high coercive field limits the application of HfO$_2$-based ferroelectric thin films in TC-type FeRAM. First, a high coercive electric field results in high application voltage and energy consumption. Second, the application voltage is close to the breakdown voltage, making the device vulnerable to breakdown and limiting the endurance and switching cycle.[107] Therefore, reducing the operating voltage and improving fatigue resistance have been some of the main research directions of HfO$_2$-based ferroelectric thin films.

The disadvantage of TC-type FeRAM are: the storage unit cannot be scaled down and destructive read out. The emergence of FeFETs solves these problems.

FeFET works by controlling the polarization charge of the ferroelectric layer through the gate voltage and thus modulating the conductivity of the transistor channel.[108] For the N-channel enhanced FeFET (Fig. 6), in the process of "writing", a positive/negative voltage higher than the coercive voltage of ferroelectric thin films is applied to the gate, resulting in the electrons/holes accumulating on the surface of p-type silicon and the transistor being in the on/off state. The on and off states of the transistor can be used to represent 0 and 1, respectively. In the process of "readout", a voltage is applied between the drain and source, and the gate is suspended. If the channel is in the "on" state, the large current passes through; otherwise, no or only the small current passes through. Thus, the storage logic data can be read by comparing the size of the output current. During the readout process, the gate remains suspended, and the polarization states of the ferroelectric film is not affected. Therefore, the "readout" operation is a nondestructive reading process. FeFET has the characteristics of nondestructive readout, high storage density, and simple structure that can be scaled down. However, due to many factors, including short storage time, poor reliability, and incompatible semiconductor processes, FeFETs have not been commercialized thus far.

According to different ferroelectric layer materials, FeFETs can be divided into PZT-based,[109] SBT-based,[110] LiNbO$_3$-based[111] and 2D van der Waals heterostructures.[112] In this article, we focus on SBT-based and HfO$_2$-based FeFETs. For the SBT-based FeFET devices, SBT thin films cannot be compatible with Si, so a buffer layer is grown on the surface of the semiconductor layer to avoid element diffusion and chemical reactions at the interface. The insertion of the buffer layer will bring about the voltage divider effect. Because the dielectric constant of the ferroelectric material (approximately 200) is larger than that of the buffer layer (a few decades), most of the voltage is applied to the buffer layer, resulting in incomplete polarization reversal, thus affecting the data storage time. The data retention time is one of the main parameters used to evaluate FeFET performance. The main factors affecting retention time are the depolarization field, gate leakage current and instability of the unsaturated hysteresis loop.[113–115] A number of attempts have been made to solve these problems, including searching for a suitable buffer layer and ferroelectric layer materials, optimizing structural parameters, and using new structures (MFMIS, ferroelectric semiconductor–FET).[115–118] A retention time of 33 days with a current rate (on/off) greater than 10^5 was observed in a self-aligned-gate Pt/SrBi$_2$Ta$_2$O$_9$/Hf–Al–O/Si FeFET, and a current rate of 10^4 was extrapolated after 10 years.[119] The memory window (MW) of the FeFET can be approximately given as $MW = 2E_c \cdot d_{Fe}$.[20] The low E_c of the SBT thin films ($2E_c < 0.1$ MV cm^{-1})[120] requires a large thickness to meet the memory window requirement,[120,121] which limits the extensibility of SBT-based FeFETs.

Compared with SBT-based ferroelectric materials, HfO$_2$-based ferroelectric materials have the advantages of a low dielectric constant, a high coercive electric field and full compatibility with CMOS technology,[122] making it more suitable for memory applications. In particular, when the ferroelectric layer thickness is decreased, the high coercivity field can compensate for the loss of the memory window so that the size of the FET can be reduced. In 2016, HfO$_2$-based FeFET was integrated into a 28 nm CMOS technology.[123] One year later, a HfO$_2$-based FeFET was successfully integrated into a 22 nm fully depleted silicon-on-insulator (FDSOI) platform, where it has been certified to have a scalability decrease to a 12 nm technology node.[124] Reducing the technology node below 10 nm requires a ferroelectric layer thickness of less than 3 nm, and the robust ferroelectricity in Hf$_{0.8}$Zr$_{0.2}$O$_2$ thin films has been demonstrated to decrease the thickness to 1 nm.[125] HfO$_2$-based materials can maintain excellent ferroelectric properties in an integrated 3D structure,[103] which makes it possible to further reduce the technology nodes of memory.

In addition, FeFET can not only be used in memory but also has wide application prospects in other fields, such as,
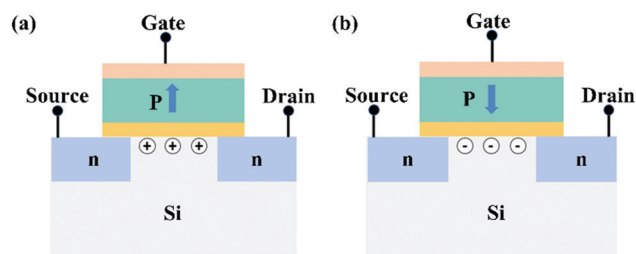

Fig. 6 Structure schematic diagram of the N-channel enhanced MFIS-type FeFET: (a) the transistor is in the off state; (b) the transistor is in the on state.

negative capacitance transistor, memristive transistors for neuromorphic computing, frequency multiplier based on FeFET, *etc.*[126–129]

3.2 Piezoelectric sensors, transducers, and actuators

Based on the piezoelectric effect (as shown in Fig. 7),[130] piezo-electric materials can realize the mutual conversion of mechanical signals and electrical signals, and are widely used in the fields of sensors, transducers and actuators.[131] With the development trend of device miniaturization and integration, MEMS, an independent intelligent system that integrates sensors, transducers, actuators and other electronics components together, has received more and more attention. Deposition of high-quality piezoelectric thin films materials is the basis for the fabrication of MEMS. Among many piezoelectric materials, perovskite-type ferroelectric thin film materials with excellent piezoelectric properties have been widely studied. In recent years, some piezoelectric devices composed of PZT thin films have been commercialized, such as inkjet printer heads and MEMS gyroscopic sensors.

The piezoelectric coefficient is one of the important parameters to characterize piezoelectric properties of materials. Improving the piezoelectric coefficient is of great practical significance for reducing the driving voltage or improving the sensitivity and accuracy of the MEMS device. Similar to bulk materials, ferroelectric thin film materials usually have excellent piezoelectric properties near MPB, so $PbZr_{0.52}Ti_{0.48}O_3$ and $PbZr_{0.53}Ti_{0.47}O_3$ thin films are the most commonly used.[131] In addition to composition, the effects of crystallographic orientation, grain size, thickness and porosity on the piezoelectric properties of materials are also explored.[132,133] Due to the hazard of Pb on environmental and human health, research on lead-free piezoelectric thin film materials has developed rapidly in recent years. Lead-free ferroelectric materials such as $Bi_{0.5}Na_{0.5}TiO_3$, $BiFeO_3$, and $K_{0.5}Na_{0.5}NbO_3$, are considered as potential candidates for MEMS.[41,134,135] In 2020, Liu *et al.* utilized Na vacancies to form nanopillars surrounded by out-of-phase boundaries in $NaNbO_3$ films, resulting in a giant electromechanical response (piezoelectric coefficient $d_{33} \sim 1098$ pm V^{-1}).[37] More details about the piezoelectric properties

and MEMS application of ferroelectric materials have been nicely reviewed by Kanno, Muralt and Malic, *et al.*[11,136–138]

Except for the piezoelectric coefficient, parameters such as electromechanical coupling coefficient, mechanical quality factor, and Curie temperature are also important parameters in practical applications. At present, most of the research on piezoelectric materials focuses on improving the piezoelectric coefficient of materials, and how to achieve the synergistic optimization of various parameters is one of the key issues to be solved. In addition, the research on the temperature stability, fatigue resistance and reliability of piezoelectric thin films is still insufficient, and further in-depth and meticulous research is required.

3.3 Energy storage capacitors

A dielectric capacitor, as an energy storage device, works through the electrostatic field generated by dielectric polarization.[139] Dielectric capacitors have drawn much attention in microelectronics and power fields due to their short charge/discharge time, high endurance and long lifetime.[140,141] The essential factors to achieve excellent performance energy storage devices are high energy storage density (ESD) and efficiency (η). The ESD and η of the dielectric capacitor can be estimated by the P–E curve. Fig. 8 shows the P–E hysteresis loops for dielectric materials and the calculation equation is as follows:[139]

$$\text{ESD} = \int_{P_{\max}}^{-P_r} E d_P$$

$$\eta = \frac{\text{ESD}}{\text{ESD} + \text{Loss}} \times 100\%$$

Thus, antiferroelectrics and relaxor ferroelectrics with high P_s, high breakdown electric field and low P_r are considered the most suitable materials for energy storage applications.[142,143] The breakdown strength of the bulk is lower than that of thin films, which results in a smaller ESD;[144] therefore, it is supposed that great energy storage properties can be obtained in the films. According to the composition, capacitors can be divided into Pb-based and lead-free capacitors.[22,145] Due to
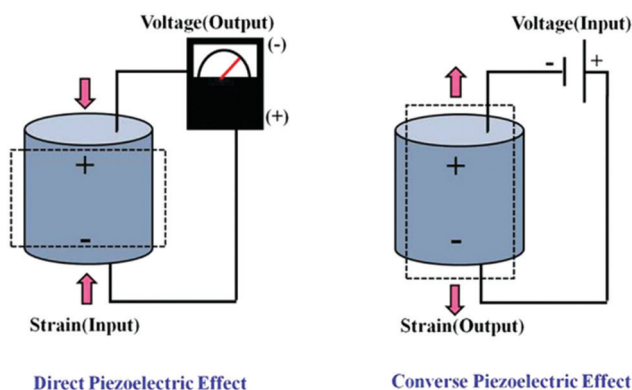

Fig. 7 Schematic diagram of the positive piezoelectric effect and the inverse piezoelectric effect.[130]

Fig. 8 The recoverable energy storage density and loss from P–E loops of a dielectric capacitor.[139]

the high ESD and efficiency, Pb-based capacitors have been studied intensively for decades, and many works have been published.[146] The Mn-doped $Pb_{0.91}La_{0.09}Zr_{0.65}Ti_{0.35}O_3$ relaxor ferroelectric thin films exhibit an ESD of 30.8 J cm^{-3} and η 68.4%.[147] Nonetheless, because lead is harmful to the human body and the environment, lead-free energy storage devices have attracted more attention.[140] Lead-free capacitors with energy storage performance comparable to, or even superior to, Pb-based capacitors have been fabricated.[148] For instance, Pan et al. achieved high ESD (112 J cm^{-3}) and η (80%) in BFO–BTO–STO solid solution thin films by designing a polymorphic nanodomain structure.[26] A superparaelectric relaxor ferroelectric thin film (Sm-doped BFO–BTO) with ultrahigh EDS of 152 J cm^{-3} and η over 70% was fabricated by Pan et al.[25] Since the volume and mass of the substrate is much larger than the film, so the total stored energy in ferroelectric film capacitors is much lower than that in ceramics. At present, factors hindering the commercialization of ferroelectric energy storage capacitors include: low energy density and total energy, small effective energy storage volume, poor temperature and fatigue stability, etc.

3.4 Ferroelectric photovoltaic devices

With the increasing demand for energy, it is urgent to develop and utilize clean renewable energy-solar energy. Photovoltaic technology is an important technical means to transform solar energy into electric energy. The working principle of photovoltaic devices is shown in Fig. 9. The electron–hole pairs are created in the material illuminated by sunlight, and the separation of electron–hole pairs produces a potential difference at both ends of the material.[149] In order to achieve high power output, high photovoltage, photocurrent and photoelectric conversion efficiency are necessary for photovoltaic devices. The high open circuit voltage (V_{oc} is not limited by its own band gap), good light absorption characteristics and favorable polarity structure for photogenerated carrier separation make ferroelectric photovoltaic materials have promising application prospects in solar cells.[149–151] The high P_r value and low band gap (2.1–2.7 eV) make BFO thin film materials one of the most promising candidate materials in the field of photovoltaics.[152–154]

Although the photovoltaic effect mechanism of ferroelectric thin film materials has not been fully understood so far, a large

number of studies have found that many factors can affect the photovoltaic effect of thin film materials, such as (i) Band gap: the narrow band gap and large absorption coefficient enable the BFO film to absorb more photons, thus producing a greater photocurrent.[155,156] In 2014, Nechache et al. proposed a new strategy to tune the bandgap of double perovskite Bi_2FeCrO_6 thin films by regulating the cationic ordering, achieving a conversion efficiency of 8.1% in multilayer devices.[157] (ii) P_r value: the larger P_r values of ferroelectric thin films can separate photogenerated carriers more effectively;[31,158] (iii) Schottky barrier height: the Schottky barrier height can be modulated by changing the electrode type or polarization state, and the high Schottky barrier height facilitates the separation of photogenerated carriers;[159,160] (iv) Conductivity: the separation of electrons and holes is a charge transfer process, so it is significant to improve the photoexcited charge transfer by balancing the ferroelectricity and conductivity of ferroelectric thin films,[161] etc. Paillard et al. published a review describing the development of ferroelectric photovoltaic materials and discussing several critical issues and parameters that require further exploration.[162] Although much research on ferroelectric photovoltaic devices has been carried out, the photovoltaic efficiency of ferroelectric thin film photovoltaic devices is too low and there is still much more to explore before commercialization.

3.5 Tunable microwave devices

The tunable microwave devices fabricated by electrically tunable dielectric materials, such as tunable oscillators, phase shifters and resonators, have wide application prospects in the field of radar and communication.[163,164] In the past few decades, a number of tunable microwave devices integrated with $Ba_{1-x}Sr_xTiO_3$ (BST) thin films have been fabricated, such as, a tunable band-stop resonator consisting of a high-temperature superconductor and BST bilayer[163] and phase array systems with enhanced performance fabricated by microwave phase shifters.[165] The key factors to the high performance of tunable microwave devices are high dielectric tunability $\left(\eta = \dfrac{\varepsilon_0 - \varepsilon_E}{\varepsilon_0}\right)$ and low dielectric loss. Ferroelectric materials, especially BST thin films, with strong electrically manipulated dielectric permittivity and low dielectric loss have made them excellent alternatives for tunable microwave devices.[166,167] Many investigations have been performed to improve the tunable properties of thin films. The dielectric loss of the BST thin film can be reduced by element doping (Co, Al, Mg, etc.), but the tunability is also weakened.[168–170] The tunability of the SBT film can be improved by applying epitaxial strain, which induces an increase in the Curie temperature.[9,54] However, due to strain relaxation, epitaxial strain cannot be maintained in the thick films required for microwave devices. In 2012, Lee et al. reported a nanocomposite ferroelectric thin film composed of BST and Sm_2O_3 which has an enhanced tunability (75%) and reduced dielectric loss (< 0.01), indicating great potential for application in electrically tunable microwave devices.[10,66]
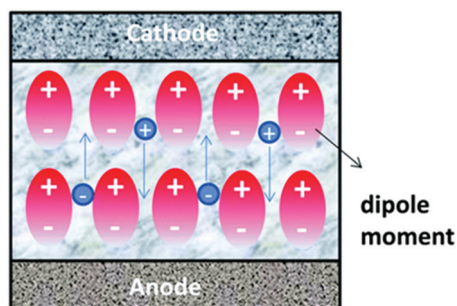
Fig. 9 The working principle of ferroelectric photovoltaic devices.[149]

3.6   Other application fields

In addition to the above applications, ferroelectric thin film materials can also be utilized to fabricate other devices. Such as, resistive RAM based on high/low resistance switching behavior, magnetoelectric RAM based on the magnetoelectric coupling effect, detectors based on pyroelectric effects, refrigeration devices based on the electrocaloric effect, *etc.*[10,171]

4. Flexible ferroelectric devices

With the rapid development of the artificial intelligence industry and wearable electronics, higher requirements are put forward for the portability and flexibility of electronic equipment,[172,173] which are difficult to meet using traditional rigid electronic devices. Hence, flexible multifunctional devices with good ductility and resilience have drawn increasing attention. Currently, nanogenerators, sensors, energy harvesting devices, and information storage devices have been fabricated by depositing polymer materials and oxide materials onto flexible substrates.[174–177] Compared with polymer materials, oxide materials generally have better physical properties and superior chemical and thermal stability, which have greater advantages in the preparation and application of devices. As mentioned above, among the many functional materials, inorganic ferroelectric thin film materials have been widely used in information storage, piezoelectric devices, optoelectronics and other fields because of their excellent electrical and optical properties. Achieving the flexibility of inorganic ferroelectric thin films can further transfer the performance advantages of these materials into flexible electronic devices. Therefore, flexible inorganic ferroelectric thin film materials are very potential candidates for flexible electronic devices. Meanwhile, flexible ferroelectric devices have become a new direction for the application and development of ferroelectric thin film materials. In this section, we briefly introduce the fabrication processes and the application prospects of flexible inorganic ferroelectric thin films.

4.1   Fabrication processes of flexible thin films

4.1.1   Direct growth methods. It is a simple and feasible strategy to grow thin films directly on malleable substrates to achieve flexible devices. Metal foil and polymers are the most common flexible substrates, both of which are malleable.[178,179] High temperature resistance allows metal foil substrates to be directly applied to the high temperature environment of ferroelectric film growth. However, the large roughness of the metal foil substrates (dozens of nanometers) and the element diffusion at the interface between the substrate and ferroelectric film will affect the performance of the flexible ferroelectric film, so a buffer layer ($LiNiO_3$, NiO, *etc.*) is usually grown on the surface of the substrate to reduce the influence of substrate roughness and element diffusion.[180,181] For example, flexible PZT thin films with high piezoelectric (140 pC N^{-1}) and pyroelectric (50 nC cm^{-2} K^{-1}) properties were prepared on malleable Ni–Cr metal foil substrates with a $LaNiO_3$ buffer layer and

can be used to fabricate piezoelectric–pyroelectric nanogenerators.[182] Polyimide (PI) substrates are more malleable than metal foil and can fit perfectly on the body. However, the low melting point ($< 400\ °C$) limits the application of flexible PI substrates, and how to make ferroelectric crystals at low temperature is a current research challenge. Bretos *et al.* proposed several novel approaches to induce PZT and BFO thin films deposited on PI substrates to crystallize at low temperature, but the P_r values of the grown flexible PZT and BFO thin films are lower than those of the films that crystallize at high temperatures.[183–185] In addition to metal foil and PI substrates, flexible ferroelectric thin films can also be deposited directly on mica substrates by van der Waals Epitaxy (vdWE), which was first proposed by Koma *et al.*[186] A series of flexible PZT and $BaTi_{0.95}Co_{0.05}O_3$ thin films have been successfully grown on mica substrates with a buffer layer,[187–189] which demonstrates that high-quality epitaxy flexible perovskite thin films can be grown on mica substrates. However, due to the influence of the mica crystal structure, the perovskite materials grown on the mica substrate are generally (111) oriented, and it is difficult to adjust the orientation. The excellent characteristics make mica materials a suitable substrate for the fabrication of flexible devices,[190] for example, atomically smooth surface, high flexibility, thermal stability and chemical inertness; the mica material is non-toxic and has good biocompatibility; the thermal expansion coefficient of mica matches that of silicon and mica is compatible with current Si-based technologies; it is compatible with current thin-film deposition techniques.

4.1.2   Stripping and transfer methods. The strategy of separating ferroelectric thin films from parent substrates and then transferring them to soft substrates has also been studied and applied extensively. There are two methods to strip thin films from parent substrates. One method is to etch the sacrificial layer.[191] The process schematic of etching the sacrificial layer to prepare flexible thin films is shown in Fig. 10a.[81] The sacrificial layer ($La_{0.7}Sr_{0.3}MnO_3$, $Sr_3Al_2O_6$) is inserted between the thin film and substrates. The etching of the sacrificial layer can separate them, and then the independent film can be transferred onto the malleable substrates to fabricate flexible films. The $La_{0.7}Sr_{0.3}MnO_3$ (LSMO) sacrificial layer can be etched with a mixture solution of KI and HCl, and the $Sr_3Al_2O_6$ (SAO) sacrificial layer can be removed by using deionized water. The water solubility of SAO reduces the etching cost and simplifies the operation, which is the sacrificial layer material commonly used in preparing flexible ferroelectric thin films.[192] Another method is the laser lift-off (LLO) process (Fig. 10b).[193,194] The separation of the ferroelectric film from the substrate can be achieved by using laser irradiation to partially vaporize the interface between ferroelectric thin films and the substrate. This method often requires the use of a wide bandgap substrate, such as a sapphire substrate.[195] Flexible ferroelectric components fabricated by the LLO process have been applied in many fields, including nanosensors and energy harvesters, *etc.*[195,196] The LLO method can achieve rapid and large-area stripping, but this method often requires the use of a wide-bandgap substrate, the cost of the laser is high, and the
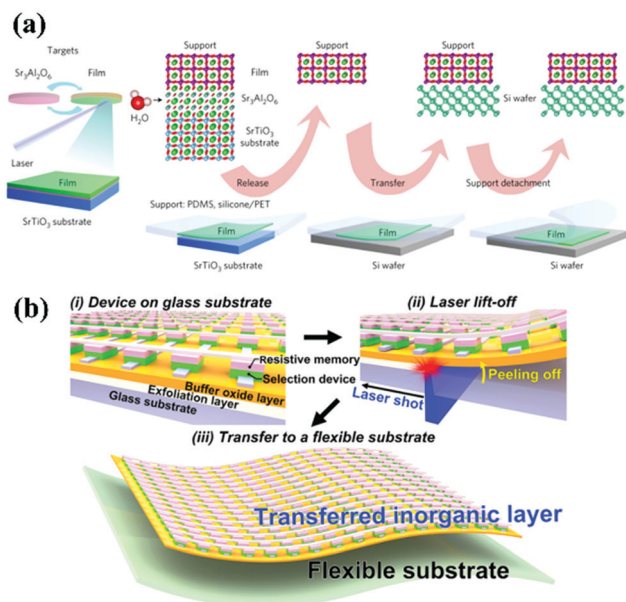
Fig. 10 (a) Process schematic of etching of the sacrificial layer to prepare flexible thin films.[81] (b) Schematic diagram of fabricating flexible thin films by a laser lift-off (LLO) process.[191]

stripping will bring thermal damage to the interface. The mature preparation process of rigid substrates is also suitable for growing ferroelectric thin films on sacrificial layers (LSMO and SAO), so sacrificial etching is an ideal method to prepare flexible ferroelectric thin films, but the few types of sacrificial layers available limit the application of this method.

4.2 Application of flexible ferroelectric thin films

4.2.1 Nonvolatile memory. To realize the application of flexible electronic devices in biomedical and industrial fields, it is necessary to develop malleable nonvolatile memory for information storage.[197] The working mechanism of flexible ferroelectric memory is the same as that of traditional ferroelectric memory, which is discussed in Section 3.1. At present, a series of flexible ferroelectric memory elements with excellent thermal and mechanical stability have been fabricated by using inorganic ferroelectric thin films.[198] A PZT-based flexible memory device was fabricated by transferring PZT thin films on a Pt-coated polyethylene terephthalate (PET) substrate through an etching sacrificial layer.[199] And the prepared memory element has a switching speed of 57 ns and retention time of more than 10 years. The P_r value of the flexible HfO_2 thin films remains nearly unchanged after 1000 cycles of the bending test with a bending radius less than 8 mm.[200] And integrating a HfO_2 thin film as a gate material on a flexible substrate resulted in a vertically flexible FeFET with an extrapolated memory window of 2.3 V after 10 years. Making use of PZT thin films as the gate materials, Tsai *et al.* fabricated a flexible FeFET on a muscovite substrate.[201] All the device characteristics, including endurance, retention time, nondestructive readout, and on/off ratio, of the flexible FeFET are not degraded after the bending test with a bending radius of 5 nm. A flexile mica/SRO/$BaTi_{0.95}Co_{0.05}O_3$/Au

capacitor displays bipolar resistive switching behavior with a high/low resistance ratio of 50 and can be used to develop a resistive memory device.[189] The high/low resistance ratio of the memory device with a 2.2 mm bending radius did not exhibit an obvious change after experiencing 360000 writing/erasing cycles. These works show the great potential of inorganic ferroelectric thin films in flexible memory devices.

4.2.2 Piezoelectric energy harvester and flexible sensors. Energy harvesters that can transform mechanical energy to electrical energy show the potential of being self-powered microelectronic devices.[196,202,203] Piezoelectric energy harvesters have received much attention since Wang and Song fabricated piezoelectric nanogenerators utilizing ZnO nanowire arrays.[204] Piezoelectric energy harvesters, known as piezoelectric nanogenerators (NG), work by the piezoelectric effect of the materials.[205] The inherent piezoelectric properties of ferroelectric materials allow for the mutual conversion of mechanical and electrical energy, but the application of traditional ferroelectric materials in energy harvester equipment is limited by their rigidity, and flexible ferroelectric thin films with excellent ductility and flexibility are the most suitable materials for fabricating energy harvester devices.[174,206] Park *et al.* successfully transferred the Au/BTO/Pt architecture onto a flexible plastic substrate by an etching process and connected them by interdigitated electrodes (IDE).[207] During periodic deformation and recovery, the nanogenerator can produce an output voltage of 1 V, a current density of 0.19 μA cm^{-2}, and a power density of 7 Mw cm^{-3}. Whereafter, Park *et al.* fabricated a highly efficient and lightweight piezoelectric NG by transferring a PZT thin film onto a polyethylene terephthalate (PET) substrate *via* the LLO process.[208] Fig. 11a shows that NG can generate an output voltage of 200 V and a current density of 150 μA cm^{-2} regardless of the forward or reverse connection at a bending strain of 0.386%. With a slight bending motion, the NG generated a current of 8.7 μA, which can light up 105 blue LEDs without any external power supply (Fig. 11b), realizing a self-powered light emitting system. Yang *et al.* fabricated lead-free piezoelectric NG by transferring $Ba_{0.85}Ca_{0.15}Zr_{0.1}Ti_{0.9}O_3$ (BCZT) films deposited on mica onto PET substrates.[209] The output voltage of this NG increased with increasing bending angle and approaches 6.7 V when the bending angle reached 90°. And this NG can charge a capacitor *via* mechanical stimulation and shows potential application prospects in the field of self-powered devices. Hwang *et al.* fabricated a flexible energy harvester by transferring single crystalline PMN–PT thin films onto a PET substrate;[210] the maximum output current was 145 μA, and the output voltage was 8.2 V, respectively. Experiments have demonstrated that the energy harvester can be used as a sustainable energy source to charge the batteries, and stimulate the heart by using artificial cardiac pacemakers (Fig. 11c). At present, many implanted medical devices require regular battery replacement, which places an economic burden on patients and a possible risk of inflammation; therefore, the development of self-powered energy harvesters has high practical significance.
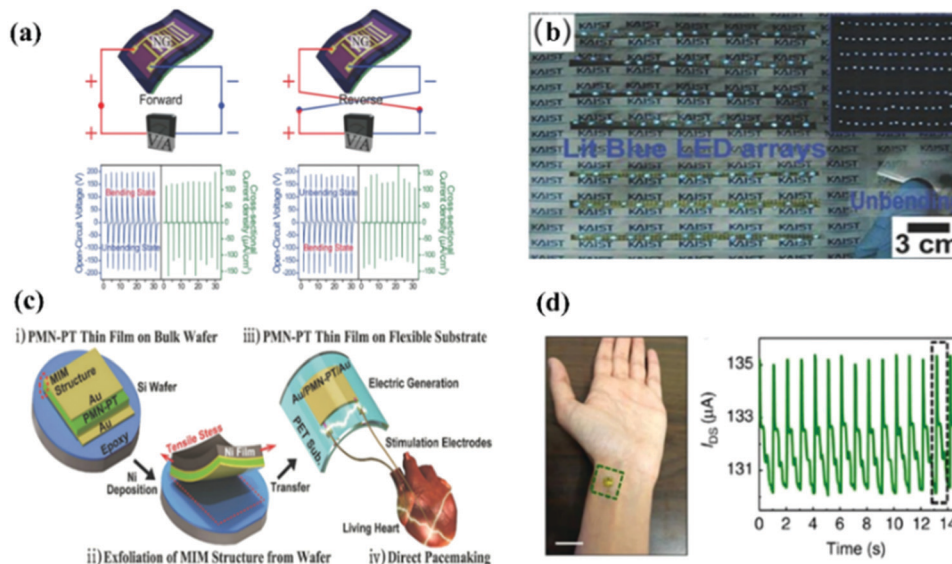
Fig. 11 (a) The output voltage and current density of PZT thin film nanogenerators in the forward (left) and reverse (right) connections, and (b) a snapshot shows the nanogenerators can simultaneously turn on 105 blue LEDs without any external power supply.[202] (c) Schematic diagrams of the fabrication process of flexible piezoelectric nanogenerators and the application of an artificial heart for a live rat.[203] (d) Photograph of the sensor placed on a wrist and the accordingly measured I_{DS}−time curves.[204]

The inherent piezoelectric properties of flexible ferroelectric thin films can also be used to fabricate flexile nano sensors. As shown in Fig. 11d,[204] Dagdeviren *et al.* fabricated a PZT-based flexible sensor that can convert skin pressure to a current output *via* capacitance coupling, with low hysteresis, fast response time (0.1 ms) and high sensitivity (0.005 Pa). Lee *et al.* reported a PZT-based flexible piezoelectric acoustic nano sensor and the sensor can sensitively and efficiently convert sound energy into piezoelectric signals within the audible living noise frequency range.[195] The NG can work as self-powered piezoelectric sensors.[206,211] Park *et al.* transferred a PZT thin film onto a flexile substrate to realize a self-powered flexible sensor, and the sensor has been shown to measure radial/carotid pulse signals, respiration frequency and tracheal movements.[212] Flexible nano sensors are expected to be applied in the field of wearable electronic devices and biomedical devices, such as electronic skin, health monitoring and intelligence systems, *etc.*[172,213]

Although significant progress has been made in the fabrication process of flexible inorganic ferroelectric thin films in recent years, the optimal solution between film quality, cost, and process complexity has not yet been reached, and the fabrication process needs to be improved. The thermal stability of flexible devices and the performance stability against bending need to be further studied and improved. At this stage, most of the research on flexible ferroelectric devices focuses on independent ferroelectric films or components, and there is still a lot to be done on the integration of flexible ferroelectric components and other functional components.

5. Conclusions

Ferroelectric thin film materials have been a hot topic in fundamental research and application fields for nearly one century. At present, the basic scientific research of ferroelectric thin film materials is still appealing, and some critical issues are to be thoroughly revealed, such as the size effect of perovskite ferroelectrics, the ferroelectricity origin of hafnium oxide-based materials, topological structures, strain engineering, interface effects, *etc.* How to derive good-performance and large-scale thin films to construct commercial devices remains to be further investigated. The preparation and research of ferroelectric thin film materials are mostly limited in the laboratory, and some fabrication methods are not suitable for large-scale commercial production. Industrial fabrication and integration process of ferroelectric thin-film devices need improvement. Moreover, there is still an urgent need to find lead-free alternatives to PZT with suitable cost and good performance.

Conflicts of interest

There are no conflicts of interest to declare.

Acknowledgements

References

1 M. E. Lines and A. M. Glass, *Principles and applications of ferroelectrics and related materials*, Oxford university press, 2001.

2 K. Seshan, *Handbook of thin film deposition techniques principles, methods, equipment and applications*, CRC Press, 2nd edn, 2002.

3 J. E. Crowell, *J. Vac. Sci. Technol., A*, 2003, **21**, S88–S95.

4 E. Subbarao and G. Shirane, *J. Chem. Phys.*, 1960, **32**, 1846–1851.

5 H. N. Lee, D. Hesse, N. Zakharov and U. Gosele, *Science*, 2002, **296**, 2006–2009.

6 Y. Sakashita, T. Ono, H. Segawa, K. Tominaga and M. Okada, *J. Appl. Phys.*, 1991, **69**, 8352–8357.

7 R. J. Zeches, M. D. Rossell, J. X. Zhang, A. J. Hatt, Q. He, C.-H. Yang, A. Kumar, C. H. Wang, A. Melville, C. Adamo, G. Sheng, Y. H. Chu, J. F. Ihlefeld, R. Erni, C. Ederer, V. Gopalan, L. Q. Chen, D. G. Schlom, N. A. Spaldin, L. W. Martin and R. Remesh, *Science*, 2009, **326**, 977–980.

8 N. Izyumskaya, Y.-I. Alivov, S.-J. Cho, H. Morkoç, H. Lee and Y.-S. Kang, *Crit. Rev. Solid State Mater. Sci.*, 2007, **32**, 111–202.

9 K. J. Choi, M. Biegalski, Y. Li, A. Sharan, J. Schubert, R. Uecker, P. Reiche, Y. Chen, X. Pan, V. Gopalan, L Chen, D Schlom and C Eom, *Science*, 2004, **306**, 1005–1009.

10 L. W. Martin and A. M. Rappe, *Nat. Rev. Mater.*, 2016, **2**, 1–14.

11 I. Kanno, *Jpn. J. Appl. Phys.*, 2018, **57**, 040101.

12 H. Takasu, *J. Electroceram.*, 2000, **4**, 327–338.

13 H. N. Lee, H. M. Christen, M. F. Chisholm, C. M. Rouleau and D. H. Lowndes, *Nature*, 2005, **433**, 395–399.

14 M. Dawber, N. Stucki, C. Lichtensteiger, S. Gariglio, P. Ghosez and J. M. Triscone, *Adv. Mater.*, 2007, **19**, 4153–4159.

15 E. Bousquet, M. Dawber, N. Stucki, C. Lichtensteiger, P. Hermet, S. Gariglio, J.-M. Triscone and P. Ghosez, *Nature*, 2008, **452**, 732–736.

16 A. Yadav, C. Nelson, S. Hsu, Z. Hong, J. Clarkson, C. Schlepütz, A. Damodaran, P. Shafer, E. Arenholz, L. Dedon, D. Chen, A. Vishwanath, A. Minor, L. Chen, J. Scott, L. Martin and R. Ramesh, *Nature*, 2016, **530**, 198–201.

17 S. Das, Y. Tang, Z. Hong, M. Gonçalves, M. McCarter, C. Klewe, K. Nguyen, F. Gómez-Ortiz, P. Shafer, E. Arenholz, V. Stoica, S. Hsu, B. Wang, C. Ophus, J. Liu, C. Nelson, S. Saremi, B. Prasad, A. Mei, D. Schlom, J. Íñiguez, P. García-Fernández, D Muller, L. Chen, J. Junquera, L. Martin and R. Ramesh, *Nature*, 2019, **568**, 368–372.

18 P. Zubko, J. C. Wojdeł, M. Hadjimichael, S. Fernandez-Pena, A. Sené, I. Luk'yanchuk, J.-M. Triscone and J. Íñiguez, *Nature*, 2016, **534**, 524–528.

19 T. Böscke, J. Müller, D. Bräuhaus, U. Schröder and U. Böttger, *Appl. Phys. Lett.*, 2011, **99**, 102903.

20 T. Mikolajick, S. Slesazeck, M. H. Park and U. Schroeder, *MRS Bull.*, 2018, **43**, 340–346.

21 F. Ali, X. Liu, D. Zhou, X. Yang, J. Xu, T. Schenk, J. Müller, U. Schroeder, F. Cao and X. Dong, *J. Appl. Phys.*, 2017, **122**, 144105.

22 F. Ali, D. Zhou, M. Ali, H. W. Ali, M. Daaim, S. Khan, M. M. Hussain and N. Sun, *ACS Appl. Electron. Mater.*, 2020, **2**, 2301–2317.

23 M. Yang, S. Li, Y. Wang, H. Qi, K. Lin, Q. Li and X. Xing, *Inorg. Chem. Front.*, 2021, **8**, 5124–5129.

24 D. Mukherjee, M. Hordagoda, D. Pesquera, D. Ghosh, J. L. Jones, P. Mukherjee and S. Witanachchi, *Phys. Rev. B*, 2017, **95**, 174304.

25 H. Pan, S. Lan, S. Xu, Q. Zhang, H. Yao, Y. Liu, F. Meng, E.-J. Guo, L. Gu and D. Yi, *Science*, 2021, **374**, 100–104.

26 H. Pan, F. Li, Y. Liu, Q. Zhang, M. Wang, S. Lan, Y. Zheng, J. Ma, L. Gu and Y. Shen, *Science*, 2019, **365**, 578–582.

27 Z. Pan, P. Wang, X. Hou, L. Yao, G. Zhang, J. Wang, J. Liu, M. Shen, Y. Zhang and S. Jiang, *Adv. Energy Mater.*, 2020, **10**, 2001536.

28 L. You, F. Zheng, L. Fang, Y. Zhou, L. Z. Tan, Z. Zhang, G. Ma, D. Schmidt, A. Rusydi and L. Wang, *Sci. Adv.*, 2018, **4**, eaat3438.

29 Q. Zhang, *J. Phys. D: Appl. Phys.*, 2003, **37**, 98–101.

30 T. Kijima, T. Aoyama, H. Miyazawa, Y. Hamada, K. Ohashi, M. Nakayama, E. Natori and T. Shimoda, *Jpn. J. Appl. Phys.*, 2005, **44**, 267–274.

31 L. Zhang, J. Chen, L. Fan, Z. Pan, J. Wang, K. Ibrahim, J. Tian and X. Xing, *J. Alloys Compd.*, 2018, **742**, 351–355.

32 J. K. Kim, S. S. Kim, W.-J. Kim, A. S. Bhalla and R. Guo, *Appl. Phys. Lett.*, 2006, **88**, 132901.

33 L. Zhang, J. Chen, H. Zhao, L. Fan, Y. Rong, J. Deng, R. Yu and X. Xing, *Appl. Phys. Lett.*, 2013, **103**, 082902.

34 Y. Wang, H. Zhao, K. Lin, J. Deng, J. Chen and X. Xing, *Inorg. Chem. Front.*, 2018, **5**, 1156–1161.

35 M. Hoffmann, U. Schroeder, C. Künneth, A. Kersch, S. Starschich, U. Böttger and T. Mikolajick, *Nano Energy*, 2015, **18**, 154–164.

36 T. Li, S. Deng, H. Liu, S. Sun, H. Li, S. Hu, S. Liu, X. Xing and J. Chen, *Adv. Mater.*, 2021, **33**, 2008316.

37 H. Liu, H. Wu, K. P. Ong, T. Yang, P. Yang, P. K. Das, X. Chi, Y. Zhang, C. Diao and W. K. A. Wong, *Science*, 2020, **369**, 292–297.

38 L. Zhang, J. Chen, J. Cao, D. He and X. Xing, *J. Mater. Chem. C*, 2015, **3**, 4706–4712.

39 Q. Zhang and R. Whatmore, *J. Phys. D: Appl. Phys.*, 2001, **34**, 2296–2301.

40 S. B. Seshadri, M. M. Nolan, G. Tutuncu, J. S. Forrester, E. Sapper, G. Esteves, T. Granzow, P. A. Thomas, J. C. Nino and T. Rojac, *Sci. Rep.*, 2018, **8**, 1–13.

41 C.-J. Cheng, D. Kan, V. Anbusathaiah, I. Takeuchi and V. Nagarajan, *Appl. Phys. Lett.*, 2010, **97**, 212905.

42 S. Fujino, M. Murakami, V. Anbusathaiah, S.-H. Lim, V. Nagarajan, C. Fennie, M. Wuttig, L. Salamanca-Riba and I. Takeuchi, *Appl. Phys. Lett.*, 2008, **92**, 202904.

43 H. Zhao, J. Wang, L. Zhang, Y. Rong, J. Chen, K. Ibrahim and X. Xing, *Dalton Trans.*, 2013, **42**, 10358–10364.

44 Y.-H. Lin, J. Yuan, S. Zhang, Y. Zhang, J. Liu, Y. Wang and C.-W. Nan, *Appl. Phys. Lett.*, 2009, **95**, 033105.

45 Y. Wang, H. Zhao, L. Zhang, Z. Liu, J. Chen, J. Deng, J. Wang, K. Ibrahim, N. I. Ilinykh and X. Xing, *Inorg. Chem. Front.*, 2016, **3**, 1473–1479.

46 J. Hao, Y. Zhang and X. Wei, *Angew. Chem., Int. Ed.*, 2011, **50**, 6876–6880.

47 G. Bai, W. Jie, Z. Yang and J. Hao, *J. Appl. Phys.*, 2015, **118**, 183110.

48 I. Ponomareva and L. Bellaiche, *Phys. Rev. Lett.*, 2008, **101**, 197602.

49 Y. Wang, H. Zhao, L. Zhang, J. Chen and X. Xing, *Phys. Chem. Chem. Phys.*, 2017, **19**, 17493–17515.

50 W. Merz, *Phys. Rev.*, 1950, **78**, 52–54.

51 G. Samara, *Phys. Rev.*, 1966, **151**, 378–386.

52 A. Goswami and L. Cross, *Phys. Rev.*, 1968, **171**, 549–550.

53 A. A. J. P. T. R. S. L. Griffith, *Philos. Trans. R. Soc., A*, 1920, **221**, 163–198.

54 D. G. Schlom, L.-Q. Chen, C.-B. Eom, K. M. Rabe, S. K. Streiffer and J.-M. Triscone, *Annu. Rev. Mater. Sci.*, 2007, **37**, 589–626.

55 A. R. Damodaran, J. C. Agar, S. Pandya, Z. Chen, L. Dedon, R. Xu, B. Apgar, S. Saremi and L. W. Martin, *J. Phys.: Condens. Matter*, 2016, **28**, 263001.

56 J. Hwang, Z. Feng, N. Charles, X. R. Wang, D. Lee, K. A. Stoerzinger, S. Muy, R. R. Rao, D. Lee and R. Jacobs, *Mater. Today*, 2019, **31**, 100–118.

57 C. Ederer and N. A. Spaldin, *Phys. Rev. Lett.*, 2005, **95**, 257601.

58 J. Haeni, P. Irvin, W. Chang, R. Uecker, P. Reiche, Y. Li, S. Choudhury, W. Tian, M. Hawley and B. Craigo, *Nature*, 2004, **430**, 758–761.

59 Y. Wei, P. Nukala, M. Salverda, S. Matzen, H. J. Zhao, J. Momand, A. S. Everhardt, G. Agnus, G. R. Blake and P. Lecoeur, *Nat. Mater.*, 2018, **17**, 1095–1100.

60 H. W. Jang, S. H. Baek, D. Ortiz, C. M. Folkman, R. R. Das, Y. H. Chu, P. Shafer, J. X. Zhang, S. Choudhury, V. Vaithyanathan, Y. B. Chen, D. A. Felker, M. D. bIEgalski, M. S. Rzchowski, X. Q. Pan, D. G. Schlom, L. Q. chen, R. Remesh and C. B. Eom, *Phys. Rev. Lett.*, 2008, **101**, 107602.

61 J. Wang, J. Neaton, H. Zheng, V. Nagarajan, S. Ogale, B. Liu, D. Viehland, V. Vaithyanathan, D. Schlom and U. Waghmare, *Science*, 2003, **299**, 1719–1722.

62 J. Zhang, Q. He, M. Trassin, W. Luo, D. Yi, M. D. Rossell, P. Yu, L. You, C. H. Wang and C. Kuo, *Phys. Rev. Lett.*, 2011, **107**, 147602.

63 J. Zhang, B. Xiang, Q. He, J. Seidel, R. Zeches, P. Yu, S. Yang, C. Wang, Y. Chu and L. Martin, *Nat. Nanotechnol.*, 2011, **6**, 98–102.

64 Y. Liu, J. Wei, X. Lou, L. Bellaiche, J. F. Scott and B. Dkhil, *Appl. Phys. Lett.*, 2015, **106**, 032901.

65 S. A. Harrington, J. Zhai, S. Denev, V. Gopalan, H. Wang, Z. Bi, S. A. Redfern, S.-H. Baek, C. W. Bark, C.-B. Eom, Q. Jia, M. E. Vickers and J. L. MacManus-Driscoll, *Nat. Nanotechnol.*, 2011, **6**, 491–495.

66 O. Lee, S. A. Harrington, A. Kursumovic, E. Defay, H. Wang, Z. Bi, C.-F. Tsai, L. Yan, Q. Jia and J. L. MacManus-Driscoll, *Nano Lett.*, 2012, **12**, 4311–4317.

67 J. L. MacManus-Driscoll, P. Zerrer, H. Wang, H. Yang, J. Yoon, A. Fouchet, R. Yu, M. G. Blamire and Q. Jia, *Nat. Mater.*, 2008, **7**, 314–320.

68 A. Kursumovic, E. Defay, O. J. Lee, C. F. Tsai, Z. Bi, H. Wang and J. L. MacManus-Driscoll, *Adv. Funct. Mater.*, 2013, **23**, 5881–5886.

69 E. Enriquez, Q. Li, P. Bowlan, P. Lu, B. Zhang, L. Li, H. Wang, A. J. Taylor, D. Yarotski and R. P. Prasankumar, *Nanoscale*, 2020, **12**, 18193–18199.

70 A. L. Sangle, O. J. Lee, A. Kursumovic, W. Zhang, A. Chen, H. Wang and J. L. MacManus-Driscoll, *Nanoscale*, 2018, **10**, 3460–3468.

71 C.-W. Nan, G. Liu, Y. Lin and H. Chen, *Phys. Rev. Lett.*, 2005, **94**, 197203.

72 H. Zheng, J. Wang, S. Lofland, Z. Ma, L. Mohaddes-Ardabili, T. Zhao, L. Salamanca-Riba, S. Shinde, S. Ogale, F. Bai, D. Viehland, Y. Jia, D. G. Schlom, M. Wuttig, A. Roytburd and R. Remesh, *Science*, 2004, **303**, 661–663.

73 N. M. Aimon, D. H. Kim, X. Sun and C. Ross, *ACS Appl. Mater. Interfaces*, 2015, **7**, 2263–2268.

74 S. M. Stratulat, X. Lu, A. Morelli, D. Hesse, W. Erfurth and M. Alexe, *Nano Lett.*, 2013, **13**, 3884–3889.

75 L. Zhang, J. Chen, L. Fan, O. Diéguez, J. Cao, Z. Pan, Y. Wang, J. Wang, M. Kim, S. Deng, J. Wang, H. Wang, J. Deng, R. Yu, J. Scott and X. Xing, *Science*, 2018, **361**, 494–497.

76 S. Mabud and A. Glazer, *J. Appl. Crystallogr.*, 1979, **12**, 49–53.

77 Y. Wang, L. Zhang, J. Wang, Q. Li, H. Wang, L. Gu, J. Chen, J. Deng, K. Lin, L. Huang and X. Xing, *J. Am. Chem. Soc.*, 2021, **143**, 6491–6497.

78 L. Zhang, D. Zheng, L. Fan, J. Wang, M. Kim, J. Wang, H. Wang, X. Xing, J. Tian and J. Chen, *Nano Lett.*, 2019, **20**, 881–886.

79 D. Lu, D. J. Baek, S. S. Hong, L. F. Kourkoutis, Y. Hikita and H. Y. Hwang, *Nat. Mater.*, 2016, **15**, 1255–1260.

80 S. S. Hong, J. H. Yu, D. Lu, A. F. Marshall, Y. Hikita, Y. Cui and H. Y. Hwang, *Sci. Adv.*, 2017, **3**, eaao5173.

81 G. Dong, S. Li, M. Yao, Z. Zhou, Y.-Q. Zhang, X. Han, Z. Luo, J. Yao, B. Peng, Z. Hu, H. Huang, T. Jia, J. Li, W. Ren, Z. Ye, X. Ding, J. Sun, C. Nan, L. Chen, J. Li and M. Liu, *Science*, 2019, **366**, 475–479.

82 D. Ji, S. Cai, T. R. Paudel, H. Sun, C. Zhang, L. Han, Y. Wei, Y. Zang, M. Gu, Y. Zhang, W. Gao, H. Huyan, W. Guo, D. Wu, Z. Gu, E. Tsymbal, P. Wang, Y. Nie and X. Pan, *Nature*, 2019, **570**, 87–90.

83 H. Béa, B. Dupé, S. Fusil, R. Mattana, E. Jacquet, B. Warot-Fonrose, F. Wilhelm, A. Rogalev, S. Petit and V. Cros, *Phys. Rev. Lett.*, 2009, **102**, 217603.

84 T. Li, Y. Zhu, S. B. Desu, C. H. Peng and M. Nagata, *Appl. Phys. Lett.*, 1996, **68**, 616–618.

85 L. Zhang, J. Chen, H. Zhao, L. Fan, Y. Rong, J. Deng, R. Yu and X. Xing, *Dalton Trans.*, 2013, **42**, 585–590.

86 M. Calzada, M. Martin, P. Ramos, J. Mendiola, R. Sirera, M. Da Silva and J. Soares, *J. Phys. Chem. Solids*, 1997, **58**, 1033–1039.

87 Y. Wang, W. Chen, B. Wang and Y. Zheng, *Materials*, 2014, **7**, 6377–6485.

88 J. F. Scott and C. A. Paz de Araujo, *Science*, 1989, **246**, 1400–1405.

89 Y. Arimoto and H. Ishiwara, *MRS Bull.*, 2004, **29**, 823–828.

90 C. De Araujo, J. Cuchiaro, L. McMillan, M. Scott and J. Scott, *Nature*, 1995, **374**, 627–629.

91 C.-H. Yang, S.-S. Park and S.-G. Yoon, *Integr. Ferroelectr.*, 1997, **18**, 377–387.

92 L. Goux, G. Russo, N. Menou, J. G. Lisoni, M. Schwitters, V. Paraschiv, D. Maes, C. Artoni, G. Corallo, L. Haspeslagh, D. Wouters, R. Zambrano and C. Muller, *IEEE Trans. Electron Devices*, 2005, **52**, 447–453.

93 J. Ze, R. Tian-Ling, Z. Zhi-Gang, L. Tian-Zhi, W. Xin-Yi, X. Dan and L. Li-Tian, *Chin. Phys. Lett.*, 2006, **23**, 1943–1946.

94 S. Majumder, D. Agrawal, Y. Mohapatra and R. Katiyar, *Integr. Ferroelectr.*, 2000, **29**, 63–74.

95 R. Moazzami, C. Hu and W. H. Shepherd, *IEEE Trans. Electron Devices*, 1992, **39**, 2044–2049.

96 X. Meng, J. Sun, J. Yu, G. Wang, S. Guo and J. Chu, *Appl. Phys. A: Mater. Sci. Process.*, 2001, **73**, 323–325.

97 B. Nagaraj, S. Aggarwal and R. Ramesh, *J. Appl. Phys.*, 2001, **90**, 375–382.

98 H. P. McAdams, R. Acklin, T. Blake, X.-H. Du, J. Eliason, J. Fong, W. F. Kraus, D. Liu, S. Madan, T. Moise, S. Natarajan, N. Qian, Y. Qiu, K. Remack, J. Rodriguez, J. Roscher, A. Seshadri and S. Summerfelt, *IEEE J. Solid-State Circuits*, 2004, **39**, 667–677.

99 J. Rodriguez, K. Remack, J. Gertas, K. Boku, K. Udayakumar, S. Summerfelt, G. Shinn, A. Haider, S. Madan and H. McAdams, in *Reliability characterization of a Ferroelectric Random Access Memory embedded within 130 nm CMOS*, 2008 17th IEEE International Symposium on the Applications of Ferroelectrics, 2008.

100 V. K. M. V. M. Kondo, V. S. K. Singh and V. H. Ishiwara, *Fujitsu Sci. Tech. J.*, 2007, **43**, 502–507.

101 C. Huang, Z. Liao, M. Li, C. Guan, F. Jin, M. Ye, X. Zeng, T. Zhang, Z. Chen and Y. Qi, *Adv. Sci.*, 2021, **8**, 2003582.

102 N. Nagel, R. Bruchhaus, K. Hornik, U. Egger, H. Zhuang, H.-O. Joachim, T. Rohr, G. Beitel, T. Ozaki and I. Kunishima, in *New highly scalable 3 dimensional chain FeRAM cell with vertical capacitor, Digest of Technical Papers*, 2004 Symposium on VLSI Technology, 2004.

103 P. Polakowski, S. Riedel, W. Weinreich, M. Rudolf, J. Sundqvist, K. Seidel and J. Muller, in *Ferroelectric deep trench capacitors based on Al: HfO2 for 3D nonvolatile memory applications*, 2004 IEEE 6th International Memory Workshop (IMW), 2014.

104 C.-P. Yeh, M. Lisker, B. Kalkofen and E. P. Burte, *AIP Adv.*, 2016, **6**, 035128.

105 T. Francois, L. Grenouillet, J. Coignus, P. Blaise, C. Carabasse, N. Vaxelaire, T. Magis, F. Aussenac, V. Loup and C. Pellissier, in *Demonstration of BEOL-compatible ferroelectric Hf 0.5 Zr 0.5 O 2 scaled FeRAM co-integrated with 130 nm CMOS for embedded NVM applications*, 2019 IEEE International Electron Devices Meeting (IEDM), 2019.

106 M. H. Park, Y. H. Lee, T. Mikolajick, U. Schroeder and C. S. Hwang, *MRS Commun.*, 2018, **8**, 795–808.

107 S. Mueller, J. Muller, U. Schroeder and T. Mikolajick, *IEEE Trans. Device Mater. Reliab.*, 2012, **13**, 93–97.

108 S.-Y. Wu, *IEEE Trans. Electron Devices*, 1974, **21**, 499–504.

109 T.-Q. Shao, T.-L. Ren, C.-G. Wei, X.-N. Wang, C.-X. Li, J.-S. Liu, L.-T. Liu, J. Zhu and Z.-J. Li, *Integr. Ferroelectr.*, 2003, **57**, 1241–1248.

110 M. Takahashi, W. Zhang and S. Sakai, in *High-endurance ferroelectric NOR flash memory using (Ca, Sr) Bi2Ta2O9 FeFETs*, 2018 IEEE International Memory Workshop (IMW), 2018.

111 X. Chai, J. Jiang, Q. Zhang, X. Hou, F. Meng, J. Wang, L. Gu, D. W. Zhang and A. Q. Jiang, *Nat. Commun.*, 2020, **11**, 1–9.

112 M. Si, P.-Y. Liao, G. Qiu, Y. Duan and P. D. Ye, *ACS Nano*, 2018, **12**, 6700–6705.

113 J. Hoffman, X. Pan, J. W. Reiner, F. J. Walker, J. Han, C. H. Ahn and T. Ma, *Adv. Mater.*, 2010, **22**, 2957–2961.

114 X. Pan and T. Ma, *Appl. Phys. Lett.*, 2011, **99**, 013505.

115 H.-T. Lue, C.-J. Wu and T.-Y. Tseng, *IEEE Trans. Electron Devices*, 2002, **49**, 1790–1798.

116 D. Xie, Y. Luo, X. Han, T. Ren and L. Liu, *J. Appl. Phys.*, 2009, **106**, 114117.

117 X. Lu and H. Ishiwara, *J. Appl. Phys.*, 2009, **105**, 061626.

118 M. Si, A. K. Saha, S. Gao, G. Qiu, J. Qin, Y. Duan, J. Jian, C. Niu, H. Wang and W. Wu, *Nat. Electron.*, 2019, **2**, 580–586.

119 M. Takahashi and S. Sakai, *Jpn. J. Appl. Phys.*, 2005, **44**, L800–L802.

120 E. Tokumitsu, G. Fujii and H. Ishiwara, *Jpn. J. Appl. Phys.*, 2000, **39**, 2125–2130.

121 U. Schroeder, S. Slesazeck and T. Mikolajick, in *Ferroelectric-Gate Field Effect Transistor Memories*, Springer, 2016, pp. 57–72.

122 T. Böscke, J. Müller, D. Bräuhaus, U. Schröder and U. Böttger, in *Ferroelectricity in hafnium oxide: CMOS compatible ferroelectric field effect transistors*, 2011 International electron devices meeting, 2011.

123 M. Trentzsch, S. Flachowsky, R. Richter, J. Paul, B. Reimer, D. Utess, S. Jansen, H. Mulaosmanovic, S. Müller and S. Slesazeck, in *A 28 nm HKMG super low power embedded NVM technology based on ferroelectric FETs*, 2016 IEEE International Electron Devices Meeting (IEDM), 2016.

124 S. Dünkel, M. Trentzsch, R. Richter, P. Moll, C. Fuchs, O. Gehring, M. Majer, S. Wittek, B. Müller and T. Melde, in *A FeFET based super-low-power ultra-fast embedded NVM technology for 22 nm FDSOI and beyond*, 2017 IEEE International Electron Devices Meeting (IEDM), 2017.

125 S. S. Cheema, D. Kwon, N. Shanker, R. Dos Reis, S.-L. Hsu, J. Xiao, H. Zhang, R. Wagner, A. Datar, M. R. McCarter, C. R. Serrao, A. K. Yadav, G. Karbasian, C.-H. Hsu, A. J. Tan, L.-c Wang, V. Thakare, X. Zhang, A. Mehta, E. karapetrova, R. V. Chopdekar, P. Shafer, E. Arenholz, C. Hu, R. Proksch, R. Ramesh, J. Ciston and S. Salahuddin, *Nature*, 2020, **580**, 478–482.

126 J. C. Wong and S. Salahuddin, *Proc. IEEE*, 2018, **107**, 49–62.

127 A. I. Khan, A. Keshavarzi and S. Datta, *Nat. Electron.*, 2020, **3**, 588–597.

128 Z. D. Luo, M. M. Yang, Y. Liu and M. Alexe, *Adv. Mater.*, 2021, **33**, 2005620.

129 H. Mulaosmanovic, E. T. Breyer, T. Mikolajick and S. Slesazeck, *Nat. Electron.*, 2020, **3**, 391–397.

130 S. Mishra, L. Unnikrishnan, S. K. Nayak and S. Mohanty, *Macromol. Mater. Eng.*, 2019, **304**, 1800463.

131 P. Muralt, R. G. Polcawich and S. Trolier-McKinstry, *MRS Bull.*, 2009, **34**, 658–664.

132 N. Ledermann, P. Muralt, J. Baborowski, S. Gentil, K. Mukati, M. Cantoni, A. Seifert and N. Setter, *Sens. Actuators, A*, 2003, **105**, 162–170.

133 A. Matavž, A. Bradeško, T. Rojac, B. Malič and V. Bobnar, *Appl. Mater. Today*, 2019, **16**, 83–89.

134 Y. H. Jeon, E. A. Patterson, D. P. Cann, P. Mardilovich, W. Stickel and B. Gibbons, *J. Am. Ceram. Soc.*, 2013, **96**, 2172–2178.

135 S. S. Won, J. Lee, V. Venugopal, D.-J. Kim, J. Lee, I. W. Kim, A. I. Kingon and S.-H. Kim, *Appl. Phys. Lett.*, 2016, **108**, 232908.

136 P. Muralt, *J. Micromech. Microeng.*, 2000, **10**, 136–146.

137 S. Trolier-McKinstry and P. Muralt, *J. Electroceram.*, 2004, **12**, 7–17.

138 S. Zhang, B. Malič, J.-F. Li and J. J. o M. R. Rödel, *J. Mater. Res.*, 2021, **36**, 985–995.

139 H. Palneedi, M. Peddigari, G. T. Hwang, D. Y. Jeong and J. Ryu, *Adv. Funct. Mater.*, 2018, **28**, 1803665.

140 H. Zhang, T. Wei, Q. Zhang, W. Ma, P. Fan, D. Salamon, S.-T. Zhang, B. Nan, H. Tan and Z.-G. Ye, *J. Mater. Chem. C*, 2020, **8**, 16648–16667.

141 B. Chu, X. Zhou, K. Ren, B. Neese, M. Lin, Q. Wang, F. Bauer and Q. Zhang, *Science*, 2006, **313**, 334–336.

142 M. D. Nguyen, C. T. Nguyen, H. N. Vu and G. Rijnders, *J. Eur. Ceram. Soc.*, 2018, **38**, 95–103.

143 C. W. Ahn, G. Amarsanaa, S. S. Won, S. A. Chae, D. S. Lee and I. W. Kim, *ACS Appl. Mater. Interfaces*, 2015, **7**, 26381–26386.

144 Y. Tian, L. Jin, H. Zhang, Z. Xu, X. Wei, E. Politova, S. Y. Stefanovich, N. V. Tarakina, I. Abrahams and H. Yan, *J. Mater. Chem. A*, 2016, **4**, 17279–17287.

145 S. K. Thatikonda, W. Huang, X. Du, C. Yao, Y. Ke, J. Wu, N. Qin and D. Bao, *Ceram. Int.*, 2019, **45**, 23586–23591.

146 M. Ye, Q. Sun, X. Chen, Z. Jiang and F. Wang, *J. Am. Ceram. Soc.*, 2011, **94**, 3234–3236.

147 Y. Liu, X. Hao and S. An, *J. Appl. Phys.*, 2013, **114**, 174102.

148 Z. Pan, J. Ding, X. Hou, S. Shi, L. Yao, J. Liu, P. Li, J. Chen, J. Zhai and H. Pan, *J. Mater. Chem. A*, 2021, **9**, 9281–9290.

149 Y. Yuan, Z. Xiao, B. Yang and J. Huang, *J. Mater. Chem. A*, 2014, **2**, 6027–6041.

150 S. Y. Yang, J. Seidel, S. J. Byrnes, P. Shafer, C.-H. Yang, M. D. Rossell, P. Yu, Y.-H. Chu, J. Scott, J. W. Ager, L. W. Martin and R. Remesh, *Nat. Nanotechnol.*, 2010, **5**, 143–147.

151 Y. Liu, S. Wang, Z. Chen and L. Xiao, *Sci. China Mater.*, 2016, **59**, 851–866.

152 K. H. Tan, Y.-W. Chen, C. N. Van, H. Wang, J.-W. Chen, F. S. Lim, K.-H. Chew, Q. Zhan, C.-L. Wu and S.-P. Chai, *ACS Appl. Mater. Interfaces*, 2018, **11**, 1655–1664.

153 W. Ji, K. Yao and Y. C. Liang, *Adv. Mater.*, 2010, **22**, 1763–1766.

154 M. M. Seyfouri, D. J. C. R. i S. S. Wang and M. Sciences, *Crit. Rev. Solid State Mater. Sci.*, 2021, **46**, 83–108.

155 J. Zhang, P. Ma, T. Shi and X. Shao, *Thin Solid Films*, 2020, **698**, 137852.

156 J. Wang, L. Luo, C. Han, R. Yun, X. Tang, Y. Zhu, Z. Nie, W. Zhao and Z. Feng, *Materials*, 2019, **12**, 1444.

157 R. Nechache, C. Harnagea, S. Li, L. Cardenas, W. Huang, J. Chakrabartty and F. Rosei, *Nat. Photonics*, 2015, **9**, 61–67.

158 W. Pei, J. Chen, D. You, Q. Zhang, M. Li, Y. Lu, Z. Fu and Y. He, *Appl. Surf. Sci.*, 2020, **530**, 147194.

159 Y. Ukai, S. Yamazaki, T. Kawae and A. Morimoto, *Jpn. J. Appl. Phys.*, 2012, **51**, 09LE10.

160 S. Sharma, M. Tomar and V. Gupta, *Vacuum*, 2018, **158**, 117–120.

161 Z. Fan, W. Ji, T. Li, J. Xiao, P. Yang, K. P. Ong, K. Zeng, K. Yao and J. Wang, *Acta Mater.*, 2015, **88**, 83–90.

162 C. Paillard, X. Bai, I. C. Infante, M. Guennou, G. Geneste, M. Alexe, J. Kreisel and B. Dkhil, *Adv. Mater.*, 2016, **28**, 5153–5168.

163 H. Su, M. Lancaster, F. Huang and F. Wellhofer, *Microw. Opt. Technol. Lett.*, 2000, **24**, 155–158.

164 S. S. Gevorgian and E. L. Kollberg, *IEEE Trans. Microwave Theory Tech.*, 2001, **49**, 2117–2124.

165 B. Acikel, T. R. Taylor, P. J. Hansen, J. S. Speck and R. A. York, *IEEE Microw. Wirel. Compon. Lett.*, 2002, **12**, 237–239.

166 J. Pond, S. Kirchoefer, W. Chang, J. Horwitz and D. Chrisey, *Integr. Ferroelectr.*, 1998, **22**, 317–328.

167 J. Xu, W. Menesklou and E. Ivers-Tiffee, *J. Eur. Ceram. Soc.*, 2004, **24**, 1735–1739.

168 P. Joshi and M. Cole, *Appl. Phys. Lett.*, 2000, **77**, 289–291.

169 L. Xiao, K.-L. Choy and I. Harrison, *Surf. Coat. Technol.*, 2011, **205**, 2989–2993.

170 K. Chong, L. Kong, L. Chen, L. Yan, C. Tan, T. Yang, C. Ong and T. Osipowicz, *J. Appl. Phys.*, 2004, **95**, 1416–1419.

171 Z. J. Wang and Y. Bai, *Small*, 2019, **15**, 1805088.

172 S. Xu, Y. Zhang, L. Jia, K. E. Mathewson, K.-I. Jang, J. Kim, H. Fu, X. Huang, P. Chava, R. Wang, S. Bhole, L. Wang, Y. J. Na, Y. Guan, M. Flavin, Z. Han, Y. Huang and J. A. Rogers, *Science*, 2014, **344**, 70–74.

173 Y. H. Jung, S. K. Hong, H. S. Wang, J. H. Han, T. X. Pham, H. Park, J. Kim, S. Kang, C. D. Yoo and K. J. Lee, *Adv. Mater.*, 2020, **32**, 1904020.

174 M. Yao, Y. Cheng, Z. Zhou and M. Liu, *J. Mater. Chem. C*, 2020, **8**, 14–27.

175 Z. M. Tsikriteas, J. I. Roscow, C. R. Bowen and H. Khanbareh, *iScience*, 2021, **24**, 101987.

176 X. Zhang, J. Jiang, Z. Shen, Z. Dan, M. Li, Y. Lin, C. W. Nan, L. Chen and Y. Shen, *Adv. Mater.*, 2018, **30**, 1707269.

177 X. Han, X. Chen, X. Tang, Y. L. Chen, J. H. Liu and Q. D. Shen, *Adv. Funct. Mater.*, 2016, **26**, 3640–3648.

178 H. Palneedi, H. G. Yeo, G.-T. Hwang, V. Annapureddy, J.-W. Kim, J.-J. Choi, S. Trolier-McKinstry and J. Ryu, *APL Mater.*, 2017, **5**, 096111.

179 M. Tomczyk, I. Bretos, R. Jiménez, A. Mahajan, E. V. Ramana, M. L. Calzada and P. M. Vilarinho, *J. Mater. Chem. C*, 2017, **5**, 12529–12537.

180 S. S. Won, H. Seo, M. Kawahara, S. Glinsek, J. Lee, Y. Kim, C. K. Jeong, A. I. Kingon and S.-H. Kim, *Nano Energy*, 2019, **55**, 182–192.

181 W. Liang, Z. Li, Z. Bi, T. Nan, H. Du, C. Nan, C. Chen, Q. Jia and Y. Lin, *J. Mater. Chem. C*, 2014, **2**, 708–714.

182 Y. J. Ko, D. Y. Kim, S. S. Won, C. W. Ahn, I. W. Kim, A. I. Kingon, S.-H. Kim, J.-H. Ko and J. H. Jung, *ACS Appl. Mater. Interfaces*, 2016, **8**, 6504–6511.

183 I. Bretos, R. Jiménez, A. Wu, A. I. Kingon, P. M. Vilarinho and M. L. Calzada, *Adv. Mater.*, 2014, **26**, 1405–1409.

184 I. Bretos, R. Jiménez, J. Ricote, R. Sirera and M. L. Calzada, *Adv. Funct. Mater.*, 2020, **30**, 2001897.

185 Í. Bretos, R. Jiménez, J. Ricote and M. L. Calzada, *IEEE Trans. Ultrason. Eng.*, 2020, **67**, 1967–1979.

186 A. Koma and K. Yoshimura, *Surf. Sci.*, 1986, **174**, 556–560.

187 J. Jiang, Y. Bitla, C.-W. Huang, T. H. Do, H.-J. Liu, Y.-H. Hsieh, C.-H. Ma, C.-Y. Jang, Y.-H. Lai and P.-W. Chiu, *Sci. Adv.*, 2017, **3**, e1700121.

188 C. Yang, Y. Han, J. Qian and Z. Cheng, *Adv. Electron. Mater.*, 2019, **5**, 1900443.

189 Y. Yang, G. Yuan, Z. Yan, Y. Wang, X. Lu and J. M. Liu, *Adv. Mater.*, 2017, **29**, 1700425.

190 Y. Bitla and Y.-H. Chu, *FlatChem*, 2017, **3**, 26–42.

191 S. R. Bakaul, C. R. Serrao, M. Lee, C. W. Yeung, A. Sarker, S.-L. Hsu, A. K. Yadav, L. Dedon, L. You and A. I. Khan, *Nat. Commun.*, 2016, **7**, 1–5.

192 L. Han, Y. Fang, Y. Zhao, Y. Zang, Z. Gu, Y. Nie and X. Pan, *Adv. Mater. Interfaces*, 2020, **7**, 1901604.

193 S. Kim, J. H. Son, S. H. Lee, B. K. You, K. I. Park, H. K. Lee, M. Byun and K. J. Lee, *Adv. Mater.*, 2014, **26**, 7480–7487.

194 W. Wong, T. Sands and N. Cheung, *Appl. Phys. Lett.*, 1998, **72**, 599–601.

195 H. S. Lee, J. Chung, G. T. Hwang, C. K. Jeong, Y. Jung, J. H. Kwak, H. Kang, M. Byun, W. D. Kim and S. Hur, *Adv. Funct. Mater.*, 2014, **24**, 6914–6921.

196 C. K. Jeong, K.-I. Park, J. H. Son, G.-T. Hwang, S. H. Lee, D. Y. Park, H. E. Lee, H. K. Lee, M. Byun and K. J. Lee, *Energy Environ. Sci.*, 2014, **7**, 4035–4043.

197 M. T. Ghoneim and M. M. Hussain, *Electronics*, 2015, **4**, 424–479.

198 W. Xiao, C. Liu, Y. Peng, S. Zheng, Q. Feng, C. Zhang, J. Zhang, Y. Hao, M. Liao and Y. Zhou, *ACS Appl. Electron. Mater.*, 2019, **1**, 919–927.

199 S. R. Bakaul, C. R. Serrao, O. Lee, Z. Lu, A. Yadav, C. Carraro, R. Maboudian, R. Ramesh and S. Salahuddin, *Adv. Mater.*, 2017, **29**, 1605699.

200 H. Yu, C. C. Chung, N. Shewmon, S. Ho, J. H. Carpenter, R. Larrabee, T. Sun, J. L. Jones, H. Ade and B. T. O'Connor, *Adv. Funct. Mater.*, 2017, **27**, 1700461.

201 M.-F. Tsai, J. Jiang, P.-W. Shao, Y.-H. Lai, J.-W. Chen, S.-Z. Ho, Y.-C. Chen, D.-P. Tsai and Y.-H. Chu, *ACS Appl. Mater. Interfaces*, 2019, **11**, 25882–25890.

202 G. T. Hwang, V. Annapureddy, J. H. Han, D. J. Joe, C. Baek, D. Y. Park, D. H. Kim, J. H. Park, C. K. Jeong and K. I. Park, *Adv. Energy Mater.*, 2016, **6**, 1600237.

203 Y. Hu and Z. L. Wang, *Nano Energy*, 2015, **14**, 3–14.

204 X. Wang, J. Song, J. Liu and Z. L. Wang, *Science*, 2007, **316**, 102–105.

205 F. R. Fan, W. Tang and Z. L. Wang, *Adv. Mater.*, 2016, **28**, 4283–4305.

206 C. Dagdeviren, Y. Su, P. Joe, R. Yona, Y. Liu, Y.-S. Kim, Y. Huang, A. R. Damadoran, J. Xia and L. W. Martin, *Nat. Commun.*, 2014, **5**, 1–10.

207 K.-I. Park, S. Xu, Y. Liu, G.-T. Hwang, S.-J. L. Kang, Z. L. Wang and K. J. Lee, *Nano Lett.*, 2010, **10**, 4939–4943.

208 K. I. Park, J. H. Son, G. T. Hwang, C. K. Jeong, J. Ryu, M. Koo, I. Choi, S. H. Lee, M. Byun and Z. L. Wang, *Adv. Mater.*, 2014, **26**, 2514–2520.

209 S. Liu, Z. Zhang, Y. Shan, Y. Hong, F. Farooqui, F. S. Lam, W.-H. Liao, Z. Wang and Z. Yang, *Mater. Chem. Front.*, 2021, **5**, 4682–4689.

210 G. T. Hwang, H. Park, J. H. Lee, S. Oh, K. I. Park, M. Byun, H. Park, G. Ahn, C. K. Jeong and K. No, *Adv. Mater.*, 2014, **26**, 4880–4887.

211 X. Cao, Y. Xiong, J. Sun, X. Zhu, Q. Sun and Z. L. Wang, *Adv. Funct. Mater.*, 2021, **31**, 2102983.

212 D. Y. Park, D. J. Joe, D. H. Kim, H. Park, J. H. Han, C. K. Jeong, H. Park, J. G. Park, B. Joung and K. J. Lee, *Adv. Mater.*, 2017, **29**, 1702308.

213 G. T. Hwang, M. Byun, C. K. Jeong and K. J. Lee, *Adv. Healthcare Mater.*, 2015, **4**, 646–658.